THE APPLICATION OF BEAM-FORMING TECHNIQUE TO ENHANCE LOW QUALITY SEISMIC REFRACTION DATA

BY

OGAH, Arewa James, B.Sc. (Hons) Physics

Thesis submitted to the Postgraduate School, Ahmadu Bello University, in partial fulfillment of the requirements for the award of the degree of MASTER OF SCIENCE IN APPLIED GEOPHYSICS.

Department of Physics
Faculty of Science
Ahmadu Bello University
Zaria, Nigeria.

March, 1990

D E C L A R A T I O N

This is an original work carried out by the author under the supervisions of Dr. S.B. Ojo and Dr. C.O. Ajayi. The thesis has not been submitted in whatever form to any institution, organization or body for the award of any degree. The work of others is duely acknowledged and referenced.

OGAH, A.J.
Author

C E R T I F I C A T I O N

This thesis entitled "The Application of Beam-Forming Technique to Enhance Low Quality Seismic Refraction Data" by Ogah, Arewa James meets the regulation governing the award of the degree of Master of Science (Applied Geophysics) of Ahmadu Bello University, and is approved for its contribution to knowledge and literary presentation.

Dr. S. B. Ojo
Chairman, Supervisory Committee — Date: 23/7/90

Dr. C. O. Ajayi
Member, Supervisory Committee — Date: 16/7/90

Prof. J. Adetunji
Head of Department — Date: 15/7/90

Prof. D. I. Saror
Dean, Postgraduate School — Date: 12-9-90

DEDICATION

To my ambitious brother,

Mr. Samuel U. Ogah, for his interest

and support.

ACKNOWLEDGEMENT

I am greatly indebted to my Supervisor, Dr. S. B. Ojo, who, through his valuable suggestions, set the pattern and standard for this original work. I appreciate his untiring criticisms that not only enticed me to work more but also exposed me to more ideas.

Dr. C. O. Ajayi, my Co-Supervisor, is also acknowledged for his concern, encouragement and part played in correcting the original manuscripts.

The author sincerely expresses his gratitude to Dr. I. B. Osazuwa and Dr. M.N. Umego for their assistance with the use of the computer and the use of their textbooks and journals. I am grateful to Mal. D. A. Jatau, Miss Mary Momoh, Miss Emili Akubo, Mr. Sunday Ogah, Mr. V. Makinde, Mr.O. Likkason, Mr. A.B. Fagbemi, Mr. J. Egwemi, Mr. L. Yusuf and Mr. F. Joda, whose contributions in one way or the other hastened the completion of this work.

I also appreciate the company of Mr and Mrs. J. Ukoje and Mr. and Mrs. F. Egwemi that made my stay in Zaria an enjoyable one. Also worthy of my appreciation is the abled Secretary to the Head of Department of Veterinary Physiology and Pharmacology, Mr. S. O. Unwuchola.

A B S T R A C T

The beam-forming (or delay and sum) method applied to refraction data involves steering of seismic arrivals from the same refractor for coherency, summing them and taking their average to obtain a 'master trace' called the beam. Based on the basic time-distance equations of refraction semismology, the technique achieves signal-to-noise ratio improvement in the process of forming the beam. Automatic determination of apparent layerivelocities was achieved by using ranges of trial velocities, and finding the velocity which maximizes the beam energy. Corresponding intercept times **were** determined by statistical estimation.

A computer programme written to perform the beam-forming operation was tested on data consisting of noiseless synthetic data, noisy synthetic data, and real refraction data from the Kubanni Drainage Basin, Results with the syntetic data showed that errors in velocity determination varied from 0.67 - 4.20% for clean data to 1.00 - 6.00% for very noisy data; while for intercept times, corresponding errors were 0.01 - 3.00% and 5.00 - 24.00% respectively.

Results from real data collected in the Kubanni basin revealed existence of two distinct geologic interfaces separating different rock units. P-wave velocity ranges of 527 - 700 m/s and 713 - 802 m/s correspond to different mixtures of silt, sand and savannah loam, and a mixture of weathered laterite and savannah loam respectively, which form the top layers at different locations. A range of 937 - 1870 m/s corresponds to a mixture of wet sand and

clay that wholly or partly form the middle layer, while 2055 - 3663 m/s and 3810 - 4325 m/s correspond to weathered and fresh basements respectively. Correlation of the refraction results with water depths in some wells suggest that the Qquifers in the basin have P-wave velocity range of 1667 - 2417 m/s. The results also revealed that the basement depths vary between 12 m in some locations to 24m in others, and that the general direction of dip of the layers is toward the Kubanni river, although a local depression exists in the southern part of the project area.

TABLE OF CONTENTS

		Page
	Title page	i
	Declaration	ii
	Certification	iii
	Dedication	iv
	Acknowledgement	v
	Abstract	vi
	Table of Contents	viii
	List of Tables	xi
	List of Figures	xii
	List of Appendices	xiv
CHAPTER I:	INTRODUCTION	1
1.1	Introduction	1
1.2	Seismic Waves and Record Quality	2
1.3	A Review of Some Attempts to Solve Noise Problems in Seismic Prospecting	5
1.3.1	Field Techniques Aimed at Noise Suppression	5
1.3.2	Noise Suppression at the Data Processing Stage	7
1.4	Objectives of the Present Work	10
CHAPTER II:	SEISMIC REFRACTION THEORY AND THE BEAM-FORMING TECHNIQUE	11
2.1	Fundamentals of Seismic Refraction Theory	11
2.1.1	Time-Distance Relations	14
2.2	The Beam-Forming Technique	19
2.2.1	Steering Delay Concept	21
2.2.2	Computer Application	23

		Page
CHAPTER III:	TEST WITH SYNTHETIC DATA	28
3.1	Synthetic Data Generation	28
3.2	Performance Test of the Computer Programme on Two-Layer Models	30
3.2.1	The Horizontal Two-Layer Case	30
3.2.2	The Dipping Two-Layer Case	33
3.3	Performance Test of the Beam-Forming Technique on Horizontal Three-Layer Model	33
3.4	The Synthetic Beam Plots	37
3.5	Analysis with Noisy Synthetic Data	41
3.5.1	Qualitative Assessment of Variation of Beam Quality with Number of Channels	41
3.5.2	Quantitative Assessment of the Signal-to-Noise Ratio Improvements with Number of Traces	43
3.5.3	Qualitative Assessment of Variation of Beam Quality with Noise Level	45
3.6	Quantitative Assessment of Accuracy of Method in the Presence of Noise	47
CHAPTER IV:	APPLICATION OF BEAM-FORMING TECHNIQUE TO REAL DATA	50
4.1	Choice and Location of the Test Area	50
4.2	Geology of the Kubanni Drainage Basin	50
4.3	Previous Studies in the Test Area	52
4.3.1	Geophysical Work	52
4.3.2	Geological Work	54
4.4	Data Collection	54
4.4.1	Introduction	54

4.4.2	Instrumentation	55
4.4.3	The Field Work	56
4.4.4	Problems Encountered	59
4.5	Data Analysis and Interpretation	59
4.5.1	The Manual Time-Distance Plots	59
4.5.2	Typical Interpretation of the Manual T-X Plots	60
4.5.3	Application of the Beam-Forming Technique	65
4.5.4	Interpreting the Results of the Beam-Forming Computer Programme	68
4.6	Comparing Typical Manual Results with those of Beam-Forming Technique	78
CHAPTER V:	DISCUSSIONS, RECOMMENDATIONS AND CONCLUSIONS	81
5.1	Limitations of Beam-Forming Technique and Suggestions for Further Work	81
5.2	Conclusions	83
	References	85
	Appendix 'A'	88
	Appendix 'B'	94
	Appendix 'C'	95
	Appendix 'D'	96

List of Tables

			Page
3.1	:	Parameters for Horizontal Two-Layer Model	32
3.2	:	Parameters for Dipping Two-Layer MOdel	34
3.3	:	Parameters for Horizontal Three-Layer Model	36
3.4	:	Variation of S/N Improvement with number of traces	44
3.5	:	Error Variation in Layer Parameters with Signal-to-noise ratio	48
4.1	:	A typical Computer output of the field result	69

List of Figures

FIGURE			PAGE
2.1	:	Simple two-layer section with plane parallel boundaries	12
2.2	:	Models of T-X plots and the corresponding two-layer case	20
2.3	:	A Sample of Synthetic beam to illustrate the logic involved in the intercept time determination	27
3.1	:	A typical example of the synthetic section generated	29
3.2	:	Two-Layer (Synthetic) T-X plots	31
3.3	:	T-X Plot of the three-layer model	35
3.4	:	Beam plots of the horizontal two-layer model	38
3.5	:	Beam plots of the dipping two-layer model	39
3.6	:	Beam plots of the horizontal three-layer model	40
3.7	:	The Variation of beam quality with increasing number of channels	42

3.8 : Decreasing Beam quality with increasing noise level 46

4.1 : Part of the Kubanni Drainage Basin showing general layout of the seismic lines on the test field 51

4.2 : Depth to basement map of the Kubanni Basin 53

4.3 : The field set up indicating the profiling technique adopted 58

4.4 : A typical field record 61

4.5 : A sample of a good quality field record 62

4.6(a)&(b) Manual T-X plots of the field data for spreads 1 & 2 of profile M-M' 63

4.6(c)&(d) Manual T-X plots of the field data for spreads 3 & 4 of profile M-M' 64

4.7 : Manual velocity/depth section for profile M-M' 66

4.8 : Geologic section for profile S-S' 72

4.9 : Geologic section for profile SS-SS' 73

4.10 : Geologic section for profile M-M' 74

4.11 : Geologic section for profile H-H' 75

4.12 : Comparison between manual and computer determined sections 79

List of Appendices

		Page
Appendix A :	Beam-Forming Computer Programme	88
Appendix B :	Random Number Generating Computer Programme	94
Appendix C :	Signal-to-noise ratio improvement Computer Programme	95
Appendix D :	Manual T-X Plots	96

CHAPTER 1

I N T R O D U C T I O N

1.1 Introduction

The commonest mode of recording seismic refraction data in the field, particularly before the invention of the digital recording system, was in the analogue form on paper. Interpretation then consists of picking the first arrivals, making the time distance (T-X) plots and computing the necessary layer parameters for subsequent geological interpretation.

Common errors that are sometimes associated with this conventional method of interpretation are (i) incorrect picking of first arrivals, and (ii) inaccurate delineation of the different velocity segments of the T-X plots.

The incorrect picking of the first arrivals from the seismic records constitutes the main source of errors associated with the T-X plots. The difficulty in accurately picking the first arrival times arises when the quality of the seismic records is low. This quality can sometimes be so low that the first arrivals are obscured (Gelchinsky & Shitivelman, 1983). The end results may therefore be: (a) wrongly computed refractor velocities, (b) falsely shallower or deeper locations of the refractors, and (c) wrongly computed layer dips which all result in wrong interpretations.

Incorrectly drawn line of best fit through a fairly scattered set of points of the T-X graph can also lead to wrong interpretation.

The layer velocity can be abruptly high or low for a small change in orientation of the line due to the sensitive nature of the time scale relative to the distance scale.

Before discussing how these interpretation errors may be minimized, it is necessary to first of all critically review some causes of low record quality and various types of field techniques and digital processing methods involved in improving record quality.

1.2 Seismic Waves and Record Quality

Seismic waves generated using either weight-drop or hammer, dinoseis, vibroseis, or dynamite as a source of seismic energy may be recorded in analogue form after reflections or refractions at various seismic interfaces. There is no doubt that the reliability of the seismic mapping is strongly dependent upon the quality of these records. Unfortunately, the quality of seismic data is sometimes so low that interpretation is made complicated if not impossible.

The record quality is determined by the level of signal relative to noise appearing on the record; that is, the signal-to-noise ratio. Therefore, to critically look at the causes of low record quality, it suffices to define signal as any event on the seismic record from which information is extracted, and noise as consisting of all the remaining 'disturbances' (coherent and incoherent) that appear on the record. The incoherent noise waves are random in both amplitude and phase while the coherent or systematic noise waves which have some elements of repeatability are commonly

surface or near-surface waves initiated by source pulses. The low quality of the seismic records is fundamentally attributed to noise. An important question of what causes the seismic noise then arises.

Some of the attempts to answer the question include those of Howell et al (1953), and Dobrin et al (1954). These workers discovered that low-frequency and low-velocity surface waves with an amplitude level that was high compared to refracted or reflected waves would often override useful information on the records. These waves have been described as coherent noise by Dobrin (1976).

Multiples have also been described as problematic to seismic prospecting. These are events that have undergone two or more reflections, and are broadly classified into long - and short-path multiples (Telford et al, 1976). The long-path multiple has a long travel path compared to primary reflections from the same deep interfaces. On the other hand, a short-path multiple arrives very soon after the associated primary reflection. Its effect is therefore that of changing wave shape instead of producing separate event. This has been described as a common and particularly troublesome type of interference (Dobrin,1976).

Anderson & McMechan (1988) identified a form of seismic noise called stationary noise because the statistics of the noise do not change with time. They attributed the causes of this unwanted event to fixed machinery, power lines, traffic, wind, bad cable connections and instrument noise, for land

survey; and propellers, on board machinery, flow noise, waves, etc. for marine exploration.

Ghost reflection is a form of multiple reflection which also generates seismic noise. A shot fired or a wave generated at a given depth near the surface and reflected downward from the surface or a shallower reflector (for example, the base of a low-velocity layer or air-water interface) superimposes its energy on that of the wave travelling downward from the source. Ghost reflections are especially important in marine surveys because of the high reflection coefficient of the water surface.

Another troublesome type of multiple, called water reverberation, produces coherent noise. It is frequently encountered in marine work and occasionally on land (Telford et al, 1976). The reverberation is due to multiple reflections in the water layer or a high velocity layer sandwiched between two good reflectors. The large reflection coefficient at the top and bottom of these layers results in a considerable amount of energy being reflected back and forth repeatedly. Depending upon the depth of the water or the thickness of the high velocity layer, certain frequencies are enhanced, as a result, the seismic record looks very sinusoidal.

Non-repeatable random noise may be due to wind shaking a geophone or causing the roots of trees to move, thus generating seismic waves (Telford et al,1976), farm animals and even geophysical field workers.

1.3 A Review of Some Attempts to Solve Noise Problems in Seismic Prospecting

Most of the improvements that have so far been achieved in the analysis of low quality seismic data have been brought about by introducing various techniques designed for suppressing noise on the records. The techniques may be subdivided into two groups: (i) Those coupled to field techniques or set up in the recording instrument to eliminate, or at least minimize the unwanted signal; and (ii) those applied during the data processing stage.

1.3.1 Field Techniques Aimed at Noise Suppression:

A method of improving the resolution of first arrivals was given by Denham (1963). He pointed out that a signal-to-noise ratio improvement of $\sqrt{n}$ could be achieved if a single geophone at each station was replaced by a group of n similar geophones when the background noise is completely uncorrelated. Denham emphasized that if the geophone groups were properly laid out, the signal would arrive in phase at the individual geophones and the background noise would be out-of-phase. The seismic waves arriving at each of the geophones in a group can then be summed up to minimize the noise effect and give better signal-to-noise ratio than that of a single geophone. This method involves a determination of the optimum geophone spacing which requires a special field technique also explained by Denham(1963).

The use of the signal averaging system (SAS) to minimize the random noise is also common, particularly when a low source of seismic energy, such as the hammer, is used.

This method involves repeating the hammer blows many times for a particular geophone spread without moving the spread until the required number of blows have been taken. The seismic signals that arrive at each geophone from all the hammer blows are coherent while the noise is incoherent. For each of the geophones, the SAS averages the noise and the weak signals that arrive from all the hammer blows. This process, called stacking, enhances the weak primary signals from the low energy source and suppresses the random noise. However, because each spread now requires several hammer blows at the same shot point, the method has the disadvantage of being slow and also involving increased labour.

Attenuation of coherent noise can be achieved by first of all running a noise profile. The noise profile may be a small scale profile with a single geophone per trace, the geophones being spaced as closely as 1-3m over a total length of order of 300m or more. The data in the form of record sections are studied to determine the nature of the coherent events (frequencies and velocities of the coherent noise) on the record. The noise can be attenuated by spreading 16 geophones, for instance, evenly over one wavelength of the coherent noise wave train. As Dobrin (1976) puts it, the 16 geophones should be grouped into two geophone groups with each group connected in series and fed into a different amplifier and galvanometer from the other group. With this type of arrangement, containing eight geophones per group, at any given time, the horizontally travelling wave will cause upward motion in four geophones of each group and downward

motion in the other four. Because all the eight geophones are connected in series, the net noise signal will be nearly zero. This procedure greatly reduces coherent noise.

Another procedure aimed at reducing coherent or incoherent noise is the common-depth-point (CDP) shooting. The'Mayne' invented field technique (Telford et al, 1976; Mayne, 1962) was designed to cancel noise of large apparent wavelength, regardless of its origin. With the CDP shooting method, a single point is sampled many times in a reflection survey. Mayne (1962) and Dobrin (1976) give the detailed field procedure. The seismic traces corresponding to individual geophones are then stacked (as done in the normal vertical stacking procedure) to enhance the signal and cancel out the noise, thus improving the signal-to-noise ratio.

1.3.2 Noise Suppression at the Data Processing State

Ervin et al (1989) used a digital computer method that automated the processing of refraction data acquired by conventional, multichannel, seismic profiling. The method began with the determination of first arrival times and ended with a contoured velocity-depth section. They used three different computer programmes. The first called PICK, performed the most critical and difficult task of accurately determining the arrival time for each trace; the second called VELDEP, translated the time distance curve into velocities and depths; and the third interpolates depths at equal velocity interval for display as a cross section printer plot.

The PICK was used to stack corresponding traces from several shots thereby minimising random noise on the stacked traces. As stated by these authors, the algorithm does not permit application of dip correction; and plotting of depths immediately beneath the shot points by VELDEP (the velocity-depth programme) introduced some errors. These were a few out of many setbacks of this computer method given by the authors.

Frequency filtering could also be used to advantage if the noise has appreciable energy outside the principal frequency range. Very low frequency components, for instance, high energy surface waves rich in low frequencies may be filtered out during the initial recording provided the low frequencies are sufficiently separated from the primary reflection frequencies. However, the spectrum of the noise often overlaps the signal spectrum and the frequency filtering is of limited value in improving record quality.

Most seismic data contain noise that is stationary. To suppress stationary noise in seismic records, Anderson & Mc-Mechan (1988) used a technique called Noise-Adaptive filtering. They partitioned each seismic trace into two windows, the noise window before the first arrival and the data window after and including the first arrival. The noise amplitudes were scaled by a factor equal to the number of samples in the noise window. After padding and tapering to reduce edge effects, the noise and the data were Fourier transformed. The amplitude spectrum of the noise was then substracted from the amplitude spectrum of the data.

Nagative amplitudes were then replaced with zeroes. The data were then inverse Fourier transformed to get the filtered output trace. Output data would then have improved signal-to-noise ratio. The main problem associated with the Noise-Adaptive filtering method is the similarity between signal and noise spectra.

The on-going discussions have been centered around the field techniques and data processing methods designed to give improved signal-to-noise ratios on both refraction and reflection seismic records. Most of the techniques thus discussed were found successful, or at least capable of improving the record quality. Inspite of these satisfactory performances, the limitations associated with them might be serious constraints in using them. A computer processing method called beam-forming technique which consists basically of introducing relative time delays to individual seismic traces of seismic refraction spread to correct for the non-coincidence of the incidence seismic energy at the different geophones, and averaging the traces to obtain the beam, has some advantages over the above techniques. It is capable of determining layer velocities and intercept times automatically without having to use some of the special field and data processing techniques. The beam-forming technique does not need the time and energy consumming multiple hammer blows as used with the signal averaging system, or wasting explosives in multiple shot arrangement. It does not need the pre-determined optimum geophone spacing as in the geophone grouping method of Denham (1963).

It does not use complex computing technique such as in the Noise-Adaptive filtering method by Anderson & McMechan (1988). Although the beam-forming technique may not serve as a substitute to any of the techniques discussed, it could be used as an alternative to a few of them.

1.4 Objectives of the Present Work

(i) The primary objective of this work is the application of a suitable technique, the beam-forming technique, for the acquisition of accurate and reliable information from relatively noisy seismic refraction data.

(ii) It was also aimed at testing the reliability of the applied technique, the beam-forming technique, by using low-quality seismic refraction data acquired from the Kubanni Drainage Basin, Zaria. This area was chosen because results of earlier geological and geo-electrical investigations in the area exist and can be compared with the interpreted seismic refraciton data.

CHAPTER II

SEISMIC REFRACTION THEORY AND THE BEAM-FORMING TECHNIQUE

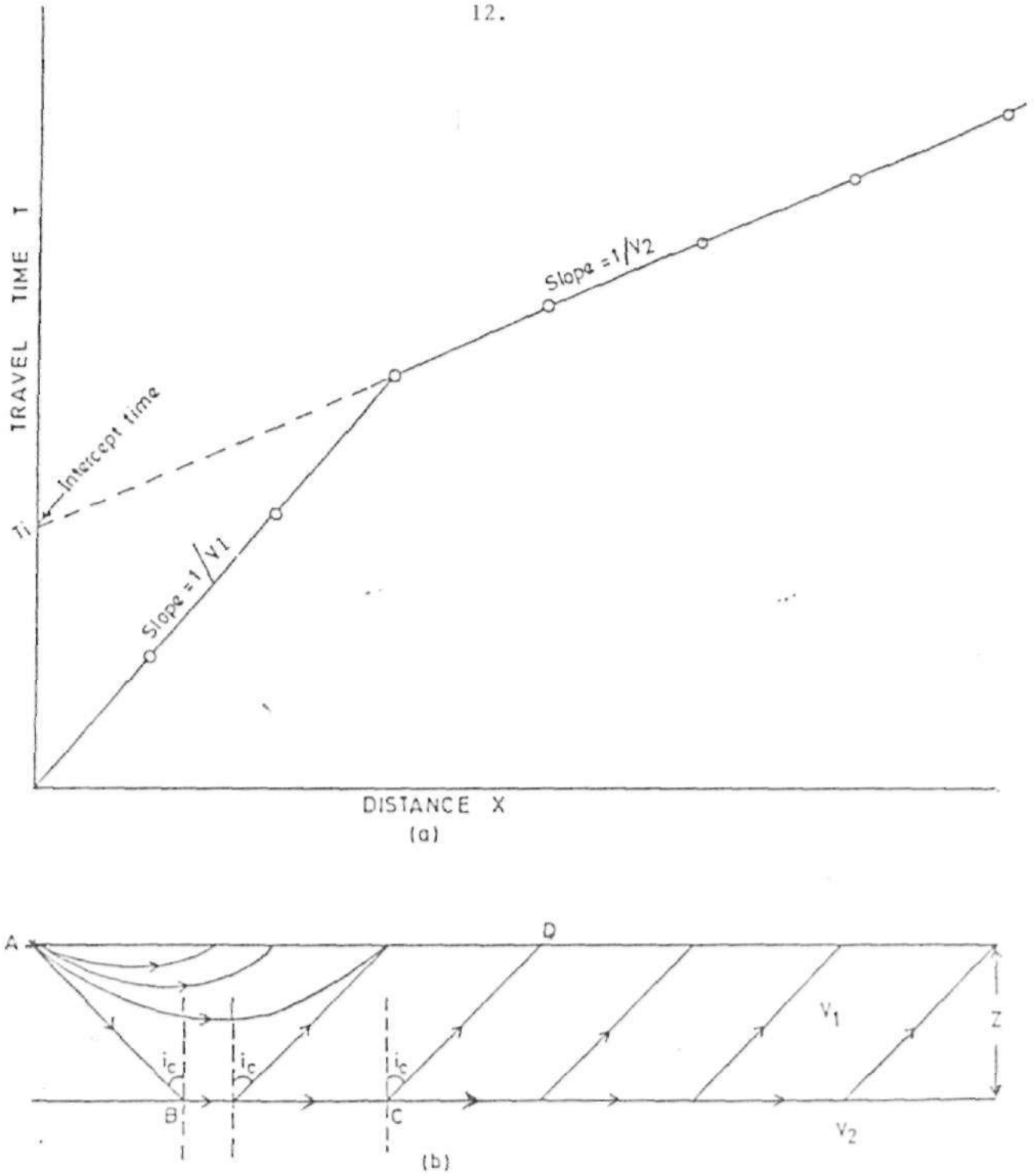
2.1 Fundamentals of Seismic Refraction Theory

To actually understand the principles involved in the beam-forming technique, a review of the fundamentals of refraction seismology is necessary.

The refraction method involves measurements (at defined locations on the surface of the ground) of travel times of seismic waves generated by an energy source. The traditional energy sources include small explosive charges and hammers. The energy is usually detected, amplified and recorded by a special equipment called the seismograph. The on-set time of the seismic waves is seen on the record of the arriving pulses. The data, when recorded in the analogue form on paper, consists of traces or seismogram corresponding to seismic wave arrivals at distances of the individual detectors from the shot point. The time-distance information obtained from these seismograms is usually converted to velocity and depths of the corresponding earth layers.

314016

The process involved in the seismic refraction method is illustrated in Figure 2.1. All the measurements are made at the surface of the ground, and the subsurface structures can be inferred from interpretation methods based on the laws of energy propagation.



$(i_c = \text{Sin}^{-1} \frac{V_1}{V_2})$

Fig. 2.1: Simple two-layer section with plane parallel boundaries:

(a) Corresponding Time-distance plot

(b) Layer model and ray paths

The propagation of seismic waves through subsurface layers is essentially the same as that of the light rays through transparent media. The refraction or angular deviation undergone by the seismic waves on passing from one layer to another depends upon the ratio of transmission velocities of the two layers. Snell's law together with the phenomenon of "critical incidence" form the physical basis of seismic refraction surveys.

When a seismic wave encounters a geologic boundary at a small angle of incidence, almost all of the compressional energy is transmitted (refracted) into the higher velocity medium (normally, the lower layer). When the incident angle exceeds the critical angle, the energy is almost totally reflected and no energy is refracted into the high-speed layer. At the critical angle, the critically refracted ray travels along the boundary between the two media at the higher of the two velocities. If the velocities of the layers increase with depth, a portion of the energy will eventually be refracted to the surface where it can be detected (See Fig. 2.1(b)).

Consider Figure 2.1 (a) in which the arrival times of the impulses are plotted against the corresponding shot-to-detector distances. The first few arrival timesare those of direct arrivals through the first layer. At some distance from the shot (corresponding to critical distance), it takes less time for the energy to travel down to the top of the second layer, refracted along the interface at the higher velocity V_2 and travel back up to the surface, than it does for the energy to travel directly through the top layer.

The straight-line through this refracted arrivals does not pass through the origin, but rather will project back to the time axis to intersect it at a time called INTERCEPT TIME, Ti. Because both the intercept time and the critical distance are directly dependent upon the velocities of the two materials and thickness of the top layer, they can be used to determine the depth to the top of the second layer.

2.1.1 Time - Distance Relations

Consider a simple two layer model similar to that of Figure 2.1 (b). The basic assumptions in obtaining the time-distance relations are that:

(i) each layer within a stratigraphic sequence is isotropic with regard to its propagation velocity.

(ii) ray paths are made up of straight-line segments, and

(iii) each layer has a higher velocity than the over-lying one.

Using the top layer velocity of V_1 in Figure 2.1(b), it is obvious that the time taken by the direct wave to travel from shot to detector is given by

$$T = X/V_1 \qquad - (2.1)$$

Where T is the travel time and X is the distance between the shot and detector.

This is represented on the T-X plot as a straight line which passes through the origin and has a scope of $1/V_1$.

Applying Snell's law to Figure 2.1(b),

$$V_1 \text{ Sin } 90° = V_2 \text{ Sin } i_c$$

So that

$$\text{Sin } i_c = \frac{V_1}{V_2} \qquad -(2.2)$$

It then follows from trigonometrical identities that

$$\text{Cos } i_c = \left(1 - \frac{V_1^2}{V_2^2}\right)^{\frac{1}{2}} \qquad -(2.3)$$

and

$$\text{Tan } i_c = \frac{V_1}{(V_2^2 - V_1^2)^{\frac{1}{2}}} \qquad -(2.4)$$

The total travel time along the refracted path ABCD is

$$T = T_{AB} + T_{BC} + T_{CD} .$$

It is therefore easy to show that

$$T = \frac{X - 2Z\,(\tan i_c)}{V_2} + \frac{2Z}{V_1 \cos i_c}$$

which becomes

$$T = \frac{X}{V_2} + \frac{2Z\,(V_2^2 - V_1^2)^{\frac{1}{2}}}{V_1\ V_2} \qquad -(2.5)$$

On substituting equations (2.3) and (2.4), where Z is thickness of the top layer.

The equation (2.5) can be rewritten as

$$T = \frac{X}{V_2} + T_i \qquad - (2.6)$$

where

$$T_i = 2Z \frac{(V_2^2 - V_1^2)^{\frac{1}{2}}}{V_1 \; V_2} \qquad - (2.7)$$

The depth is then given by,

$$Z = \frac{T_i \; V_1 \; V_2}{2(V_2^2 - V_1^2)^{\frac{1}{2}}} \qquad - (2.8)$$

The expression of the equation (2.6) can be written for any number of horizontal layers (Dobrin, 1976); for instance,

$$T = \frac{X}{V_3} + T_{i2}$$

is the same expression for a three-layer case, but with the third layer velocity V_3 and intercept time T_{i2} given (Dobrin, 1976) by

$$T_{i2} = 2Z_1 \frac{(V_3^2 - V_1^2)^{\frac{1}{2}}}{V_3 \; V_1} + 2Z_2 \frac{(V_3^2 - V_2^2)^{\frac{1}{2}}}{V_3 \; V_2} \qquad - (2.9)$$

where

Z_1 and Z_2 are the thicknesses of first and second layers respectively.

It has also been shown by Dobrin (1976) that for a dipping two-layer case, the total travel time shooting up - dip and down-dip are :

$$T_u = \frac{X}{V_1} \text{Sin}(i_c - \alpha) + \frac{2Zu \text{ Cos}i_c}{V_1} \quad - (2.10)$$

and

$$T_d = \frac{X}{V_1} \text{Sin}(i_c + \alpha) + \frac{2Z_d \text{ Cos}i_c}{V_1} \quad - (2.11)$$

respectively. Z_u and Z_d are the perpendincular distances to the interface from the shot from which arrivals are received at the up-dip and down-dip ends of line respectively.

α indicates the dip of the interface.

From the equations (2.10) and (2.11), the slopes of the refracted branch are given by:

$$M_u = \frac{\text{Sin}(i_c - \alpha)}{V_1}$$

and

$$M_d = \frac{\text{Sin}(i_c + \alpha)}{V_1}$$

for the up-dip and down-dip segments respectively. If the apparent velocities in the up-dip and down-dip directions are represented by V_u and V_d respectively, then

$$\frac{1}{V_u} = M_u = \frac{\text{Sin}(i_c - \alpha)}{V_1}$$

or

$$V_u = \frac{V_1}{\text{Sin}(i_c - \alpha)}$$

and

$$V_d = \frac{V_1}{\text{Sin}(i_c + \alpha)}.$$

Therefore,

$$\text{Sin}(i_c - \alpha) = \frac{V_1}{V_u} \quad -(2.12)$$

and $$\text{Sin}\ (i_c + \alpha\ ) = \frac{V_1}{V_d} \qquad - (2.13)$$

From equations (2.12) and (2.13), the critical angle of incidence, i_c and the dip of the interface, α can be computed. Then the true second layer velocity, V_2, for the dipping layer can be computed using the expression of equation (2.2).

It is also obvious from the equations (2.10) *and* (2.11) that the up-dip and down-dip intercept times are

$$ti_u = \frac{2Zu\ \text{Cosi}_c}{V_1} \qquad - (2.14)$$

and

$$ti_d = \frac{2Z_d\ \text{Cosi}_c}{V_1} \qquad - (2.15)$$

respectively. Therefore, from

$$Z_u = \frac{ti_u\ V_1}{2\ \text{Cosi}_c}$$

and

$$Z_d = \frac{ti_d\ V_1}{2\ \text{Cosi}_c}$$

the first bed thicknesses under up-dip and down-dip shot points can be computed.

The on-going computations can easily be done (Redpath, 1973; Dobrin, 1976) for any number of dipping layers.

2.2. The Beam-Forming Technique

Beam-forming as used here, consists basically of introducing relative time delays to the individual seismic traces of a seismic refraction spread to correct for the non-coincidence of the incident seismic energy at the different geophones, summing them up and taking the average to obtain the beam. The assumption here is that the signal is coherent between the geophones and that the noise is random or incoherent. For groups of geophones corresponding to the same refraction segments of the travel time curve, this basic assumption is valid.

The procedure involved in beam-forming technique is illustrated in Figure 2.2 in which Figure 2.2(a) shows a segment of a synthetic section generated by introducing a simple wavelet accross the velocity section shown in Figure 2.2(b). The segment corresponds to a section of the refraction branch consisting of three seismic traces. These traces can be properly aligned (Fig. 2.2(c)) by appropriately shifting their discrete amplitudes.

According to Ojo and Mereu (1983), each amplitude of the seismic trace may be represented as

$$g_{ij} = S_j + n_{ij};\ i = 1,2,\ldots, M;\ \text{and}\ j = 1,2,..,K \qquad - (2.16)$$

where g_{ij} = the j - th sample of the trace at the i - th geophone

S_j = the j - th sample of the signal

n_{ij} = the j - th sample of the noise at the i - th geophone.

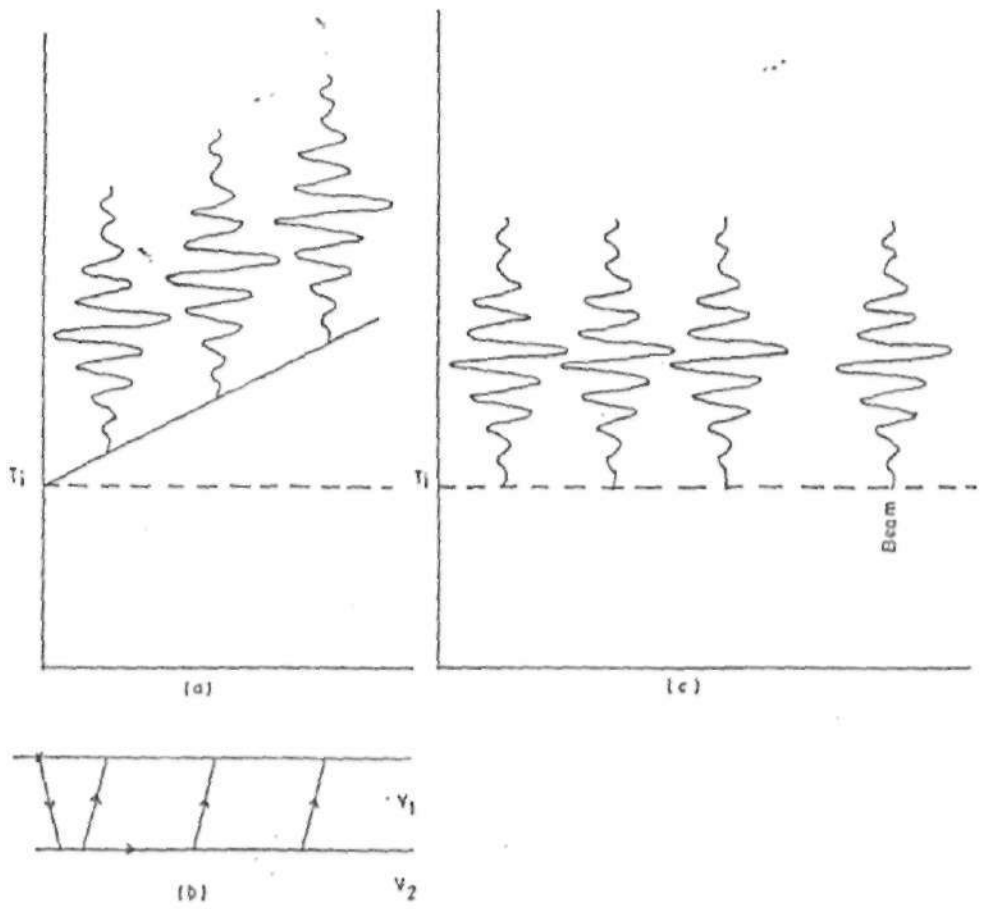


Fig. 2.2: Models of T-X plots and the corresponding two-layer case

(a) shows positions of unsteered traces
(b) Layer model
(c) shows steered traces and the beam.

K is the total number of the sampled points per trace, and M is the number of geophones in the section. The noise term consists of a random part which includes instrument generated noise and wind noise which are stationary and independent of the presence of the signal; and a signal generated component which arises as a result of incoherent energy caused by scattering by inhomogeneities along the paths.

The equation for the beam is then given (Ojo and Mereu, 1983) by

$$B_j = \frac{1}{M} \sum_{i=1}^{M} g_{ij} \qquad - (2.17)$$

or

$$B_j = S_j + \frac{1}{M} \sum_{i=1} nij \qquad - (2.18)$$

It may therefore be seen that when noise is absent as in Figure 2.2 (a), the noise term on the right hand side of equation (2.18) becomes zero and the beam is identical to each of the individual traces with the appropriate steering delay applied (Fig. 2.2 (c)). The energy of the beam (E_B), defined as the sum of the squared amplitudes of the beam, can then be expressed as

$$E_B = \sum_{j=1}^{K} B_j^2 \qquad - (2.19)$$

from Equation (2.17), where B_j indicates discrete amplitudes of the beam.

2.2.1 Steering Delay Concept

Using a simple two-layer case as an example, the steering delay can be deduced from Equation (2.6) and is seen to be given by

$$t_i = \frac{Xi}{V} \qquad - (2.20)$$

where X_i is the distance of the i-th geophone from the shot point and V is the refractor velocity. The steering delay procedure can therefore be illustrated by re-arranging Equation (2.6) such that

$$T_i = T - \frac{X}{V_2} \qquad - (2.21)$$

where $\frac{X}{V_2}$ is the same as the steering delay term of Equation (2.20). The time T taken by the seismic wave to travel from the shot point to each of the geophones increases with distance X of the geophone away from the point (Fig. 2.2(a)). To achieve the coherent arrangement of the traces (such as Figure 2.2 (c)), appropriate value of the steering delay(ti) computed for the individual traces of Figure 2.2 (a) is subtracted from the travel time T of the corresponding trace. With the signal perfectly coherent along the refraction branch and the steering delays accurately determined, the energy of the beam is equal to the energy of the individual traces. This condition is achieved when the value of V in Equation (2.20) is equal to refractor velocity.

When V is different from the refractor velocity, the traces are improperly steered and do not add up coherently when summed to get the beam. In this case, the beam energy is less than the energy of the individual traces.

This condition thus suggests a procedure for the application of the beam-forming technique. First of all, a rough estimate of the refractor velocity is determined from the T-X plot. A range of velocities centred at this first estimate is then used in applying appropriate steerings to the travel times using Equation (2.6). For each velocity used, a beam is obtained and the beam energy is calculated. The velocity which corresponds to the maximum beam energy is therefore the true refractor velocity.

On the other hand, equation (2.21) shows that when the traces are properly aligned (giving the beam of maximum energy), the intercept time., Ti, corresponds to the initial signal deflection of the formed beam (See Figure 2.2 (c)). Therefore, in picking the intercept time for any refraction segment, a search is made for this initial point of deflection.

2.2.2 Computer Application

A computer programme was written to perform the beam forming operation, and to automatically determine apparent velocities and intercept times. All computations were done using an IBM PC/AT belonging to the Physics Department, A.B.U., Zaria.

To use the computer programme, the analogue seismic traces are first converted to discrete amplitudes (each corresponding to a specific time) by digitization. The inputs into the computer programme include:

NCH - number of traces averaged to form beam

NPT - number of points used to form beam

NTRACE - the total number of sampled points per trace

DT - digitizing interval

VSTRT - initial trial velocity

VSTOP - final trial velocity

DV - velocity increment for analysis

X(I) - distance of i-th trace from shot point

TSTRT(I)- time of first non-zero amplitude on i-th trace

CHA(I) - digitizing amplitudes for i-th trace

The use of these parameters are indicated in the computer programme of Appendix A, and some in equation (2.22).

The principle involved in the computer programme is centred around equation (2.6) or (2.21). Therefore, using the input parameters to the programme listed above, equation (2.21) can be rewritten as

$$T_i = TSTRT\ (I) - \frac{X(I)}{V} \qquad - (2.22)$$

where V is the steering velocity ranging between VSTRT and VSTOP at a constant interval DV. The programme uses this range of velocities to seek a constant value T_i for all the traces belonging to the same refractor segment.

For each value of V in equation (2.22), the programme rearranges all the traces, obtains the beam and computes the beam energy. When the trial velocity (steering velocity) used is equal to the refractor velocity (as explained earlier), the programme obtains a proper arrangement of the steered traces similar to that of Figure 2.2(c), which corresponds to the beam of maximum energy. As earlier stated, the computer programme was written to pick:

(i) the apparent velocity corresponding to maximum beam energy, and

(ii) the intercept time from the beam of maximum energy.

These parameters are used on equations (2.1) through (2.15) to compute geologic layer parameters.

(i) Picking of the correct apparent velocity

A segment of the computer programme of Appendix A assumes the initial trial velocity corresponding to the first formed beam as the apparent velocity for the refractor branch. It then compares the first beam energy with the subsequent ones. A trial velocity value corresponding to beam of maximum energy is then picked as the correct apparent velocity.

(ii) Intercept time determination

The intercept time, T_i, is given (according to equation (2.20)) by

$$T_i = T - \frac{X}{V}$$

since this is an equation of a refraction branch of the T-X plot, T_i is never equal to zero (Telford et al, 1976; Dobrin, 1976).

Therefore, the beam of maximum energy is of the form shown in Figure 2.3, in which the initial part is noisy, followed by the on-set of the signal at the arrowed point. To illustrate how this arrowed point is determined, let the amplitudes of the beam be represented (as in equation (2.17)) by B_j, and the time corresponding to any value of B_j by

$$T_j; \quad \text{where } j = 1,2,\ldots., K,$$

K being the number of points used to form the beam. The time T_1 corresponding to the time at point A of the Figure 2.3 is initially taken as the intercept time for the refraction branch. If the amplitudes B_j (excluding zeroes) are of the same sign for consecutive points, $j = 1,\ldots,6$, then T_1 is the correct intercept time. If, on the other hand, any value of the B_j is zero or has different sign from the rest within this range, then the deflection on the beam at point A is attributed to noise effect, thus the choice of T_1 is wrong and the test is repeated for the next point T_2. This process is continued until a point such as the arrowed point of the Figure 2.3 is encountered. At this point, more than six consecutive non-zero values of B_j have the same sign. Therefore, the arrowed point is picked as the correct intercept time. A segment of the computer programme has been written to perform this function.



Fig. 2.3: A Sample of Synthetic beam to illustrate the logic involved in the intercept time determination

CHAPTER III

TEST WITH SYNTHETIC DATA

3.1 Synthetic Data Generation

In order to investigate the performance and feasibility of the beam-forming technique in analysing refraction data, tests were carried out with the aid of some synthetic data. The primary objective of these tests was to determine the effectiveness of the velocity and intercept time selecting procedure, and the accuracy of the automatically computed layer thicknesses and dips. To achieve this, it was considered appropriate to start from the simplest problem of analysing noiseless data since competence in this indicates a good starting point for the analysis of noisy or poor quality data.

The synthetic data was generated by assuming some layer models (both horizontal and dipping), with assumed layer velocities, thicknesses and dips (where necessary). Travel times for the models (for the refracted branch) were then computed at a set of suitable geophone distances using ray theory. A set of synthetic sections were then generated by convolving a 61ms wavelet with the spike sequence corresponding to the travel times using a sampling interval of 1 ms. The basic wavelet was selected from a field example. Figure 3.1 is a typical example of the synthetic sections generated.

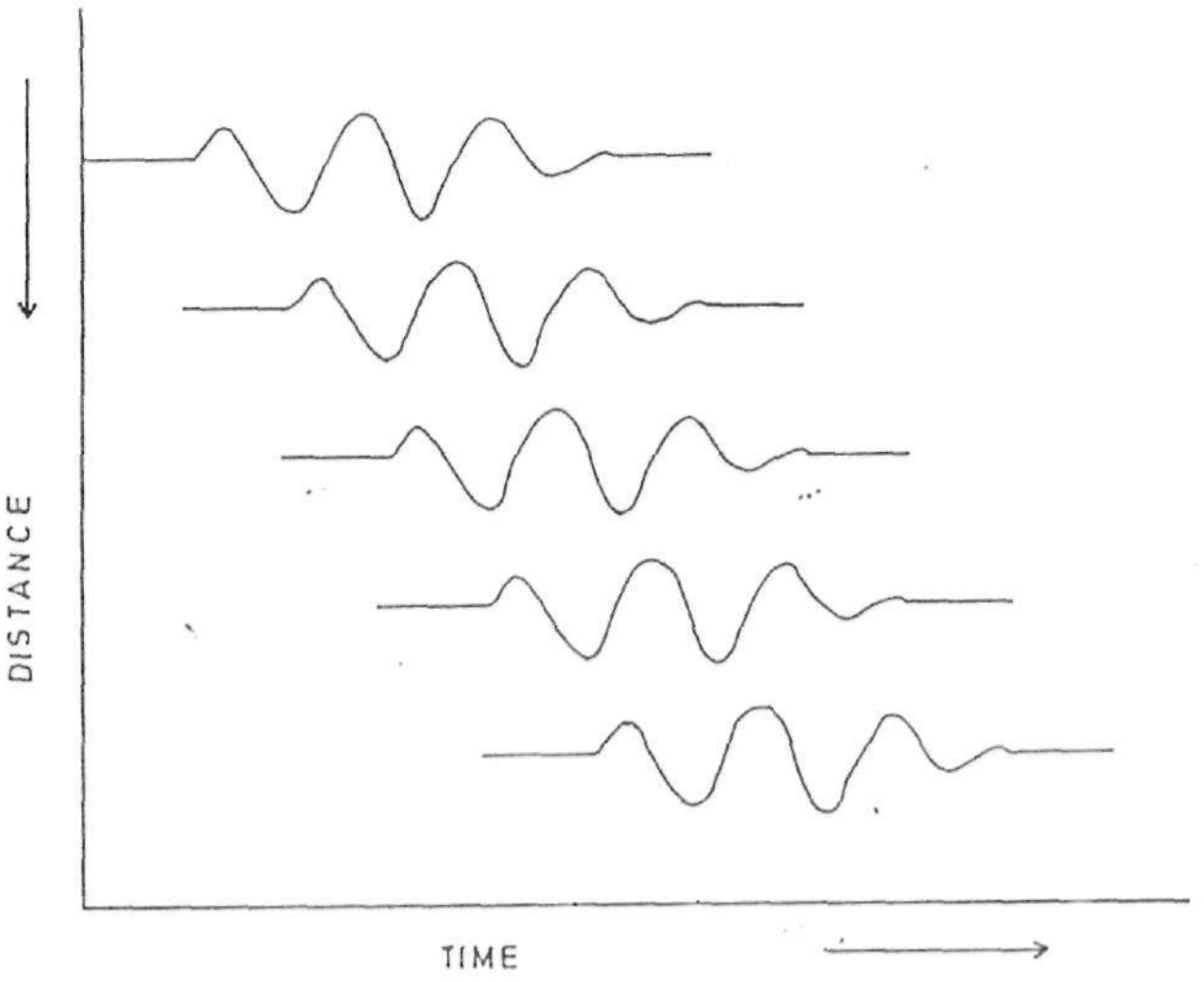


Fig. 3.1: A typical example of the synthetic Section generated

3.2 Performance Test of the Computer Programme on Two-Layer Models

Using the method of synthetic data generation already discussed, two models of the two-layer case were obtained. These were:

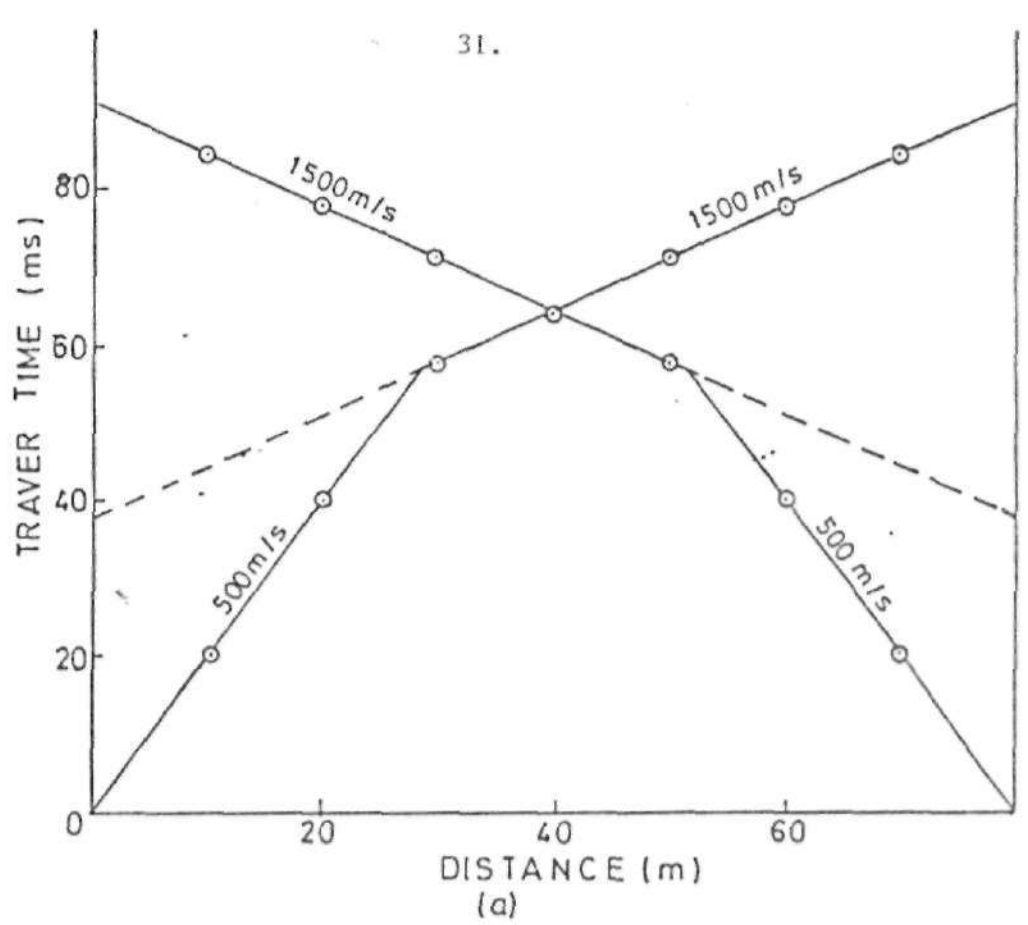
(i) a horizontal two-layer model and

(ii) a dipping two-layer model.

The performance of the computer programme on each of these models is discussed separately below.

3.2.1 The Horizontal Two-layer Case

The first and second layer velocities were chosen to be 500.0 m/s and 1500.0m/s respectively. The first layer thickness was also chosen to be 10.0m. This resulted in an intercept time of 37.7 ms (Fig. 3.2(a)). The computer programme was applied on synthetic data comprising of discrete amplitudes of the traces, appropriately selected distances of the geophones from the shot points and the first arrival times computed from the layer model. The correlation between the chosen parameters of the model and the values of the corresponding parameters obtained using the beam-forming technique are displayed in Table 3.1. The results show high performance of the technique on the noiseless data with relative percentage errors varying between 1.3% and 1.9%



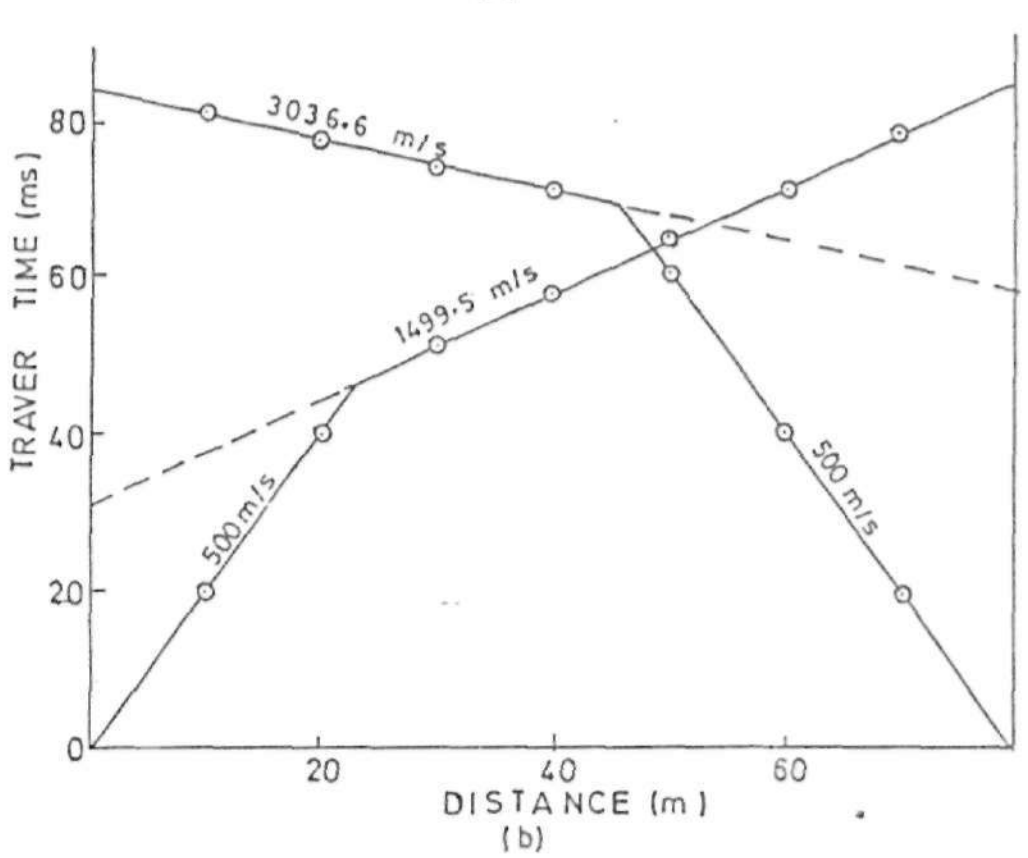


Fig. 3.2: Two-Layer (synthetic) T-X plots

(a) horizontal case, (b) dipping case

Table 3.1: Parameters for Horizontal Two-Layer Model

Parameter	True model value of parameter	Value Obtained from computer programme	Relative % error
Second layer, forward profile velocity and intercept time	1500m/s, 37.7ms	1480m/s,37.0ms	1.3, 1.9
Second layer, reverse profile velocity and intercept time	1500m/s, 37.7ms	1480m/s,37.0ms	1.3, 1.9
First layer thickness	10.0m	9.8m	2.0

3.2.2 The Dipping Two-Layer Case

The first and second layer velocities were chosen to be 500m/s and 2000m/s respectively. The layer thicknesses of 8.0m and 15m were chosen for down-dip and up-dip shot points respectively, which corresponded to a dip of 5°. Using these values of the parameters and equations (2.3), (2.10) and (2.11), the corresponding intercept times and the apparent velocities in the up-dip and down-dip directions were computed. The computer programme was then applied as earlier explained for the horizontal two-layer case. The T-X plot for the dipping model is shown in Figure 3.2(b), and a comparison between the model values of the layer parameters and the values determined from the computer programme are shown in Table 3.2. The results are also accurate with error range between 0.2% and 4.2%.

3.3 Performance Test of the Beam-Forming Technique on Horizontal Three-Layer Model

The first, second and third layer velocities were chosen to be 500.0m/s, 1500.0m/s and 3500.0m/s respectively. The thicknesses of the first and the second layers were chosen to be 8m and 15m respectively. From this, the intercept times and apparent velocities were computed using the appropriate equations. The T-X plot obtained is shown in Figure 3.3 and a comparison between the model values and the corresponding values determined from the computer programme are shown in Table 3.3, with errors varying between 0.01% and 3.3% in the computer results.

ABU BAKR LIBRARY
AHMADU BELLO UNIVERSITY

Table 3.2: Parameters for Dipping Two-Layer Model

Parameter	True Model Value of parameter	Value Obtained from computer programme	Relative % error
Second layer, forward profile: apparent velocity and intercept time	1499.5m/s,30.9ms	1450.0m/s, 30.0ms	3.3, 3.0
Second layer, reverse profile: apparent velocity and intercept time.	3036.6m/s,57.9ms	2910.0m/s,57.0ms	4.2, 1.6
Actual Second layer velocity	2000.0m/s	1927.8m/s	3.6
Up-dip thickness of first layer	15.0m	14.8m	1.3
Down-dip thickness of first layer	8.0m	7.8m	2.5
Dip	5°	4.99°	0.2

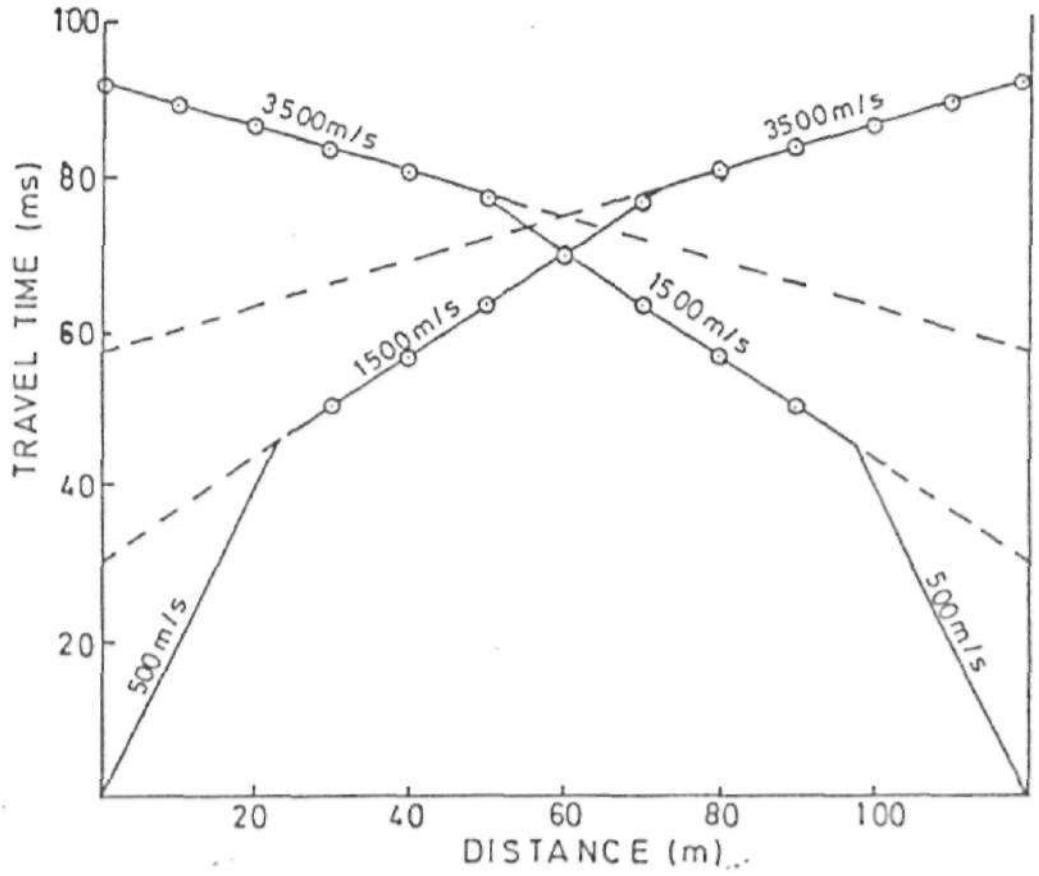


Fig. 3.3: T-X plot of the three-layer model

Table 3.3: Parameters for the Horizontal Three-Layer Model

Parameter	True Model Values of parameter	The Values Obtained from the computer programme	Relative % error
Second layer, forward profile: apparent velocity and intercept time.	1500.0m/s,30.2ms	1490.0m/s,30.0ms	0.67,0.01
Second layer, reverse profile: apparent velocity and intercept time.	1500.0m/s,30.2ms	1490.0m/s,30.0ms	0.67,0.01
Actual second layer velocity	1500.0m/s	1490.0m/s	0.67
Third layer, forward profile: apparent velocity and intercept time.	3500.0m/s,57.7ms	3530.0m/s,58ms	0.86,0.52
Third layer, reverse profile: apparent velocity and intercept time.	3500.0m/s,57.7ms	3530.0m/s,58ms	0.86,0.52
Actual third layer velocity	3500.0m/s	3530 m/s	0.86
Thickness of the first layer	8.0m	7.9m	1.25
Thickness of the second layer	15.0m	14.5m	3.33

3.4 The Synthetic Beam Plots

As earlier stated, Singh (1978) emphasized the importance of accurate intercept time determination by regarding depths as the most important information that one seeks from a seismic survey. Therefore, another significant achievement of the present application of the beam-forming technique would be the accurate determination of the intercept times. The layer depths obtained for the models of Figure 3.2 and 3.3 were found to be fairly accurate as obvious from Tables 3.1, 3.2 and 3.3. The beams formed in the process of analysing the synthetic data for the three models; that is, the horizontal two-layer, the dipping two-layer and the horizontal three-layer models are shown in Figures 3.4 to 3.6. They correspond to the T-X plot of Figure 3.2(a), 3.2(b) and 3.3 respectively.

The purpose of plotting the beam is to illustrate that the intercept times automatically determined by the computer programme of Appendix A actually correspond to the initial deflection points of the respective beams. For example, in Figure 3.4, the on-set time of the beam signal which are indicated by the arrows correspond to 37.0ms which is the intercept time automatically determined by the computer programme (Table 3.1.). Similarly, the values of 30.0ms and 57.0ms in Figure 3.5 are comparable to the computer values given in Table 3.2.

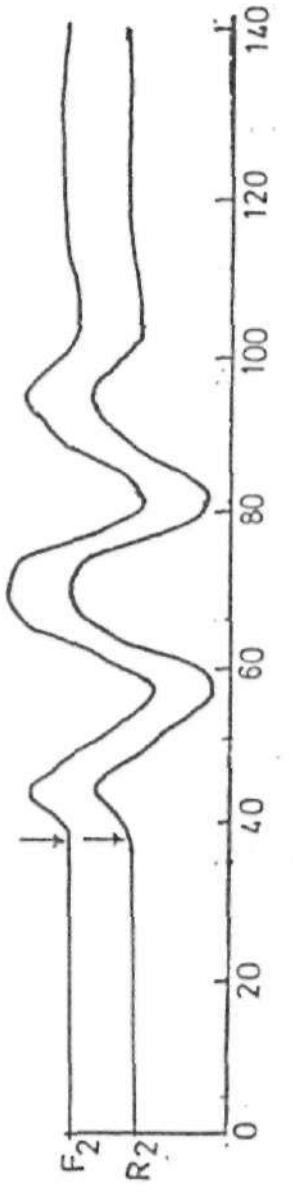


Fig. 3.4: Beam plots of the horizontal two-layer model
F & R indicate Forward and Reverse profiles respectively.
2 indicates 2nd layer
The intercept times are arrowed.

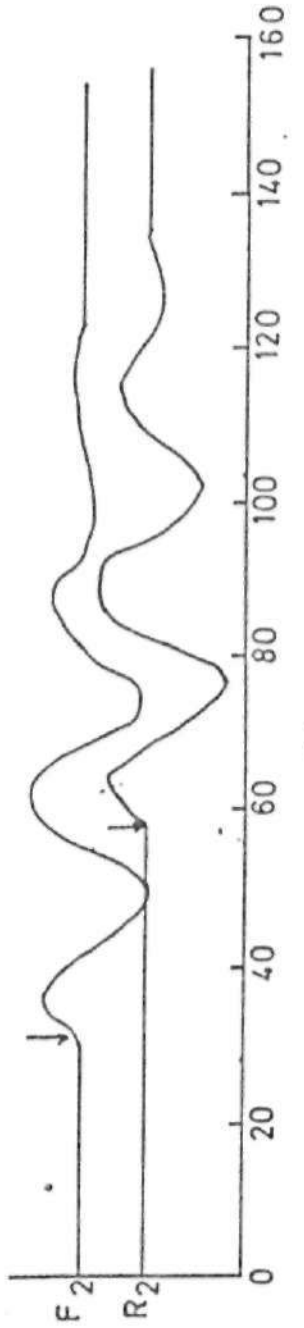


Fig. 3.5: Beam plots of the dipping two-layer model
F & R indicate forward and reverse profiles respectively
2 indicates 2nd layer
The intercept times are arrowed.

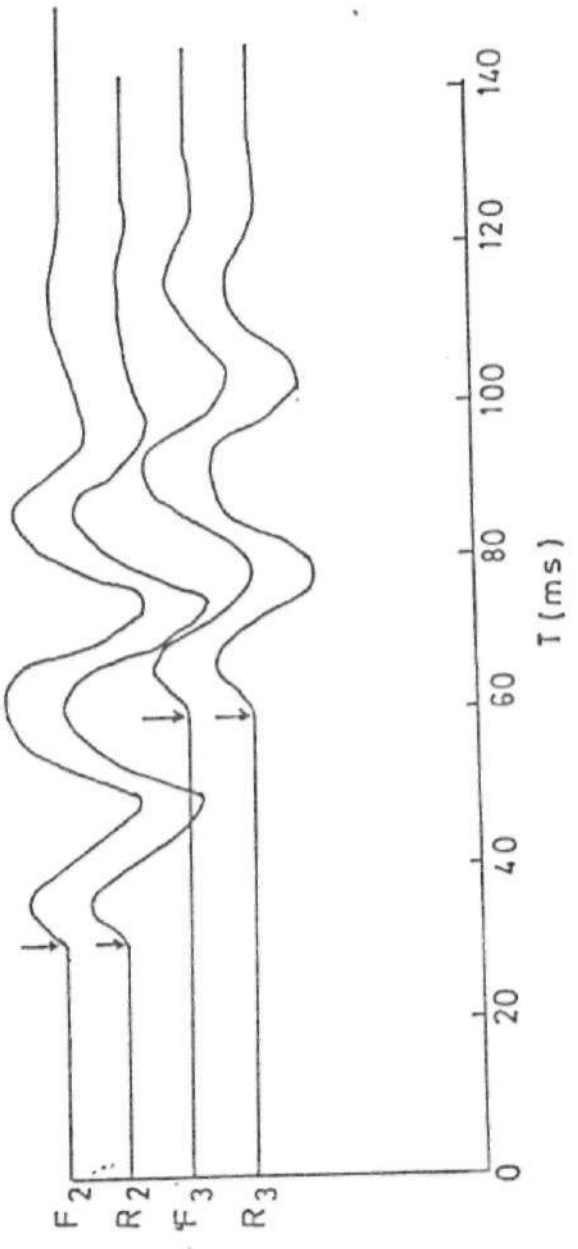


Fig. 3.6: Beam plots of the horizontal three-layer model
F & R indicate forward and reverse profiles respectively.
2 and 3 indicate 2nd & 3rd layers respectively
The intercept times have been arrowed

3.5 Analysis with Noisy Synthetic Data

A random number routine (Merchant,1979) that could generate random numbers between 0 and 1 was used (see Appendix B). This was modified to generate both negative and positive random numbers of any desired amplitude. The generated random numbers were added, where required, to the clean synthetic seismic traces to serve as noise.

3.5.1 Qualitative Assessment of Variation of Beam Quality with Number of Channels

The quality of the beam signal, the end product of the applied steering delays and summation operation performed on the noisy traces, is a function of the number of traces (Channels) used to form the beam. To take a critical look at this factor, signal-to-noise ratio was assessed qualitatively.

Different sets of the random noise were added to different traces ranging in number between two and twelve per group. In each case, the noisy traces were steered for maximum beam energy (as earlier explained). The traces and the corresponding beam were plotted. The signal-to-noise ratio improvements observed on the formed beams as the number of traces per stack increases are displayed in Figure 3.7 for four of the eleven cases investigated. It is obvious from the figure that the noise suppression increased progressively from Figure 3.7 (a) to Figure 3.7(d), evidence of the improvement in the quality of the beam with increasing number of traces.

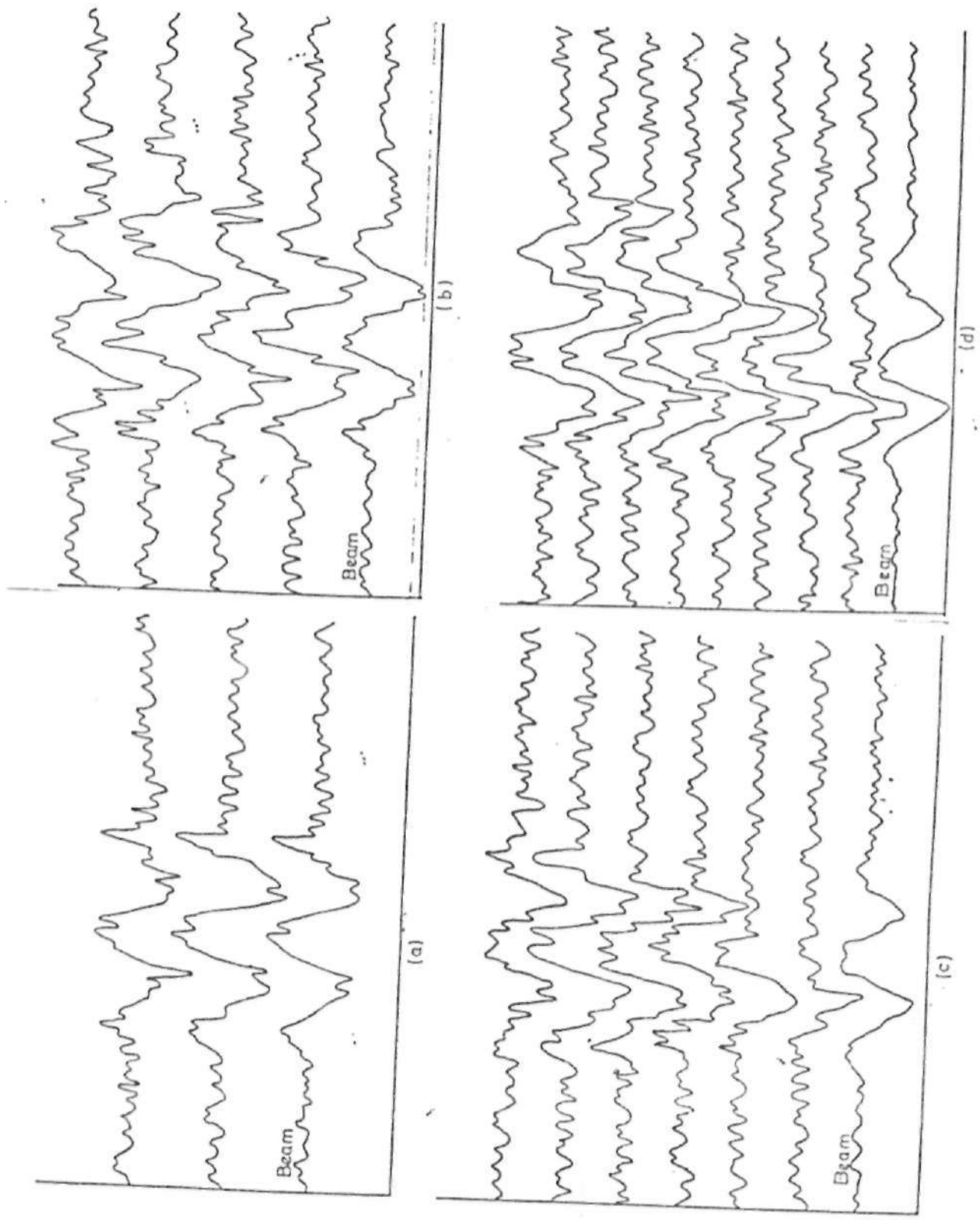


Fig. 3.7: The variations of beam quality with increasing number of channels.

3.5.2. Quantitative Assessment of the Signal - to - Noise Ratio Improvement with Number of Traces:

To test the non-correlation of the noise used for analysis, a set of random numbers generated with the routine of Appendix B were formed into noise traces. These traces were combined in groups of two to twelve. Energy content of a single noise trace and those of the summed traces were computed using the computer programme of Appendix C. Since truely random traces would add up destructively, the energy content of such added traces would be less than that for the individual trace. The Energy content of the single (uncombined) trace was therefore used to assess improvements in the signal-to-noise ratio of the combined traces. This energy was divided by the energy of each of the summed traces to obtain the corresponding improvement in signal-to-noise ratio.

Table 3.4 shows signal-to-noise ratio improvement with number of summed random traces n. It is obvious from the table that for any number of traces n, there is $\sqrt{n}$ signal - to - noise ratio improvement (gain in the amplitudes of the signal over those of the noise). This consistent

Table 3.4: Variation of S/N improvement with number of traces

Number of traces summed	Signal-to-noise ratio improvement
1	1.00
2	1.41
3	1.73
4	2.00
5	2.24
6	2.45
7	2.65
8.	2.83
9	3.00
10	3.16
11	3.32
12	3.46

variation agrees with the statistical test of randomness (Denham, 1963; Telford et al, 1976) that if the numbers are truely random, the sum of n random traces will be proportional to $\sqrt{n}$, so that the signal - to - noise ratio will be improved by $\sqrt{n}$. Therefore, the noise traces used are completely uncorrelated.

3.5.3. Qualitative Assessment of Variation of Beam Quality with Noise Level:

Another factor which affects the quality of the beam signal is the signal to noise ratio. Under normal circumstances, seismic interpretation becomes less reliable as the noise level in the survey area becomes progressively higher if no precautions are taken. In order to examine the quality of beam signal in the presence of increasing noise level, six synthetic traces were again generated, and to these were added different levels of noise. The noise amplitudes were increased in ten stages and the beam signal obtained each time. The quality of the corresponding beams was observed to decrease progressively with noise level, as shown in Figure 3.8. It can be observed that in Figure 3.8(a) the beam maintains its 'natural' quality since n noise has been added to the synthetic traces. As the noise level was increased progressively from Figure 3.8(b) to 3.8(d), the beams systematically become more distorted.

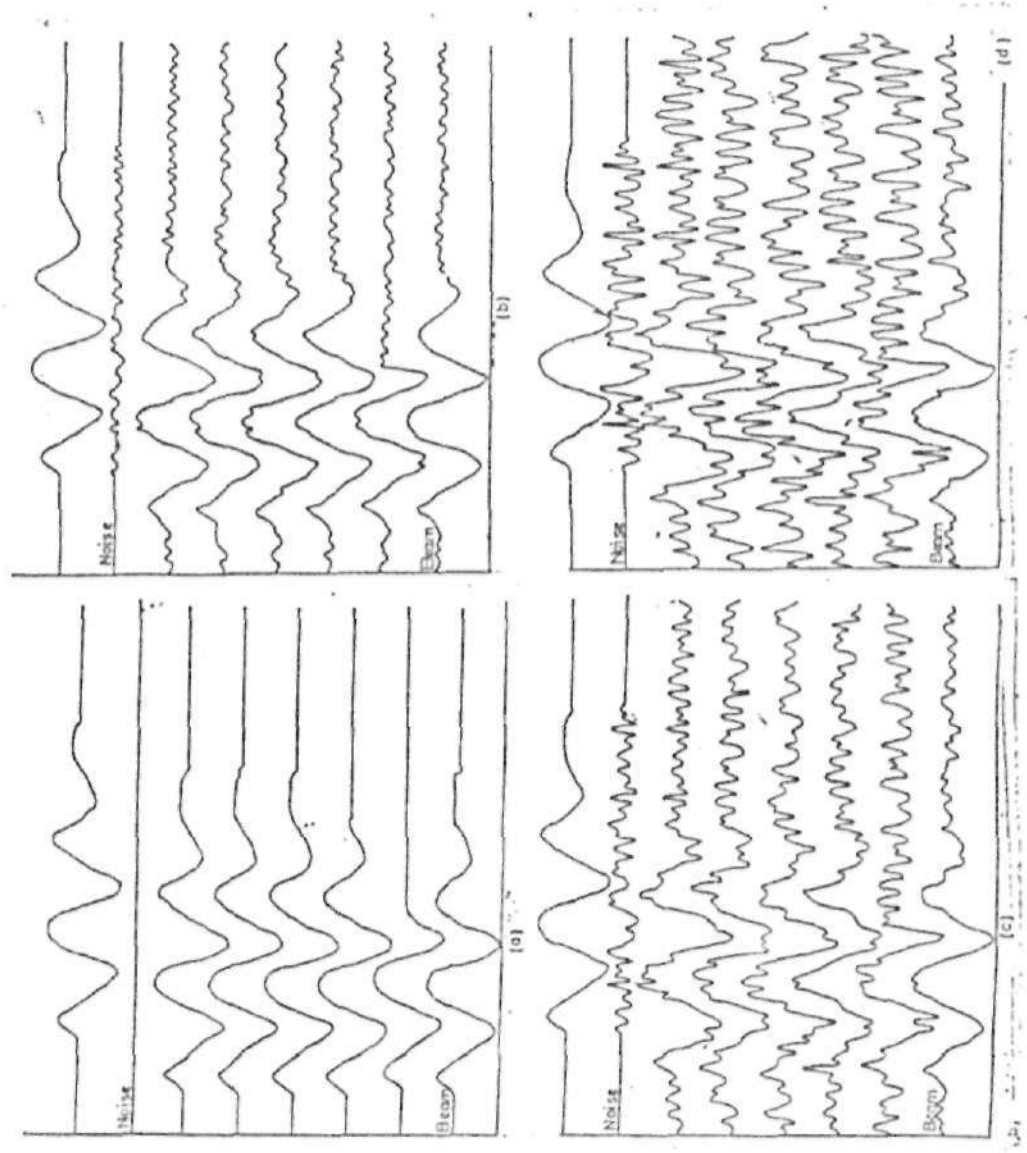


Fig. 3.8: Decreasing Beam quality with increasing noise level.

However, it can also be seen from the figures that at any noise level within the given range, the beam signal was of a better quality than each of the individual traces.

3.6 Quantitative Assessment of Accuracy of Method in the Presence of Noise:

As earlier stated, the development of a technique for the acquisition of accurate and reliable seismic refraction results from relatively noisy data is one of the primary objectives of this work. It is therefore necessary to quantitatively assess how successful the beam-forming techniques will be at doing this.

In this assessment, a simple two-layer case was again used. First and second layer velocities were chosen to be 500m/s and 1000m/s respectively for the two-layer model. A first layer thickness of 3m was also chosen. As described in chapter two, a set of synthetic traces were again generated for the model. Various levels of noise was then added to the traces before the beam-forming technique was used to interprete the synthetic data. The deviations in values of parameters computed from those of the starting model as the noise level increased or as the signal-to-noise ratio decreased was then considered a measure of the accuracy of the technique. Using these deviations, the relative percentage errors in each of the computed parameters was determined. Table 3.5 shows the values of these parameters corresponding to different signal-to-noise ratio and the relative percentage errors in each of the parameters.

Table 3.5: Error Variation in Layer Parameters with signal-to-noise ratio

Signal-to noise ratio	2nd layer velocity (m/s)	Relative error in velocity (%)±	Intercept time(ms)	Relative error in intercept time(%)±	Thick-ness of top layer (m)	Relative error in top lay thick-ness(%)±
Model Parameters	1000.00	-	10.00	-	3.00	-
2.65	1010.00	1.00	10.5	5.00	3.02	0.67
0.68	1030.00	3.00	10.80	8.00	3.09	3.00
0.17	1040.00	4.00	11.00	10.00	3.14	4.70
0.05	1060	6.00	12.40	24.00	3.52	17.33

It can be observed that as the noise level increases, the values of the layer parameters computed progressively deviated from those of the model parameters. That is, the errors in the computed parameters increased with decreasing signal-to-noise ratio (Table 3.5). The relative errors in the computed parameters shown in this table show that the result obtained with the technique from even a very low quality data is adequately reliable.

CHAPTER IV

APPLICATION OF BEAM-FORMING TECHNIQUE TO REAL DATA

4.1 Choice and Location of the Test Area

After successfully testing the beam-forming technique with synthetic data, it was then considered justified to apply the method to real seismic data. These data were collected in some selected profiles within the Kubanni Drainage Basin, Zaria. The data were obtained to determine the depth-to-basement and direction of dips of geologic layering along these profiles with the aim of comparing these parameters with previous estimates by other workers using different methods.

The Kubanni Drainage Basin is situated in the centre of the South-east quandrant of Zaria Sheet No.102 SW of Nigeria Ordinance Survey Map. The profiles on which the refraction data were collected lie within an area bounded by longitudes 7°50'E and 7°54'E, and latitudes 11°28'N and 11°31'N, and lies to the west of Ahmadu Bello University, Zaria (Fig. 4.1).

4.2 Geology of the Kubanni Drainage Basin

The Kubanni Drainage Basin is underlain by rocks of the Precambrian Basement Complex pre-dominated by biotite-gneiss (McCurry, 1970). The biotite-gneiss outcrops mainly in stream valleys where they are deeply weathered. The gneiss complex forms about 30-40% of the basement complex rocks exposures in the basin (Wright & McCurry, 1970).

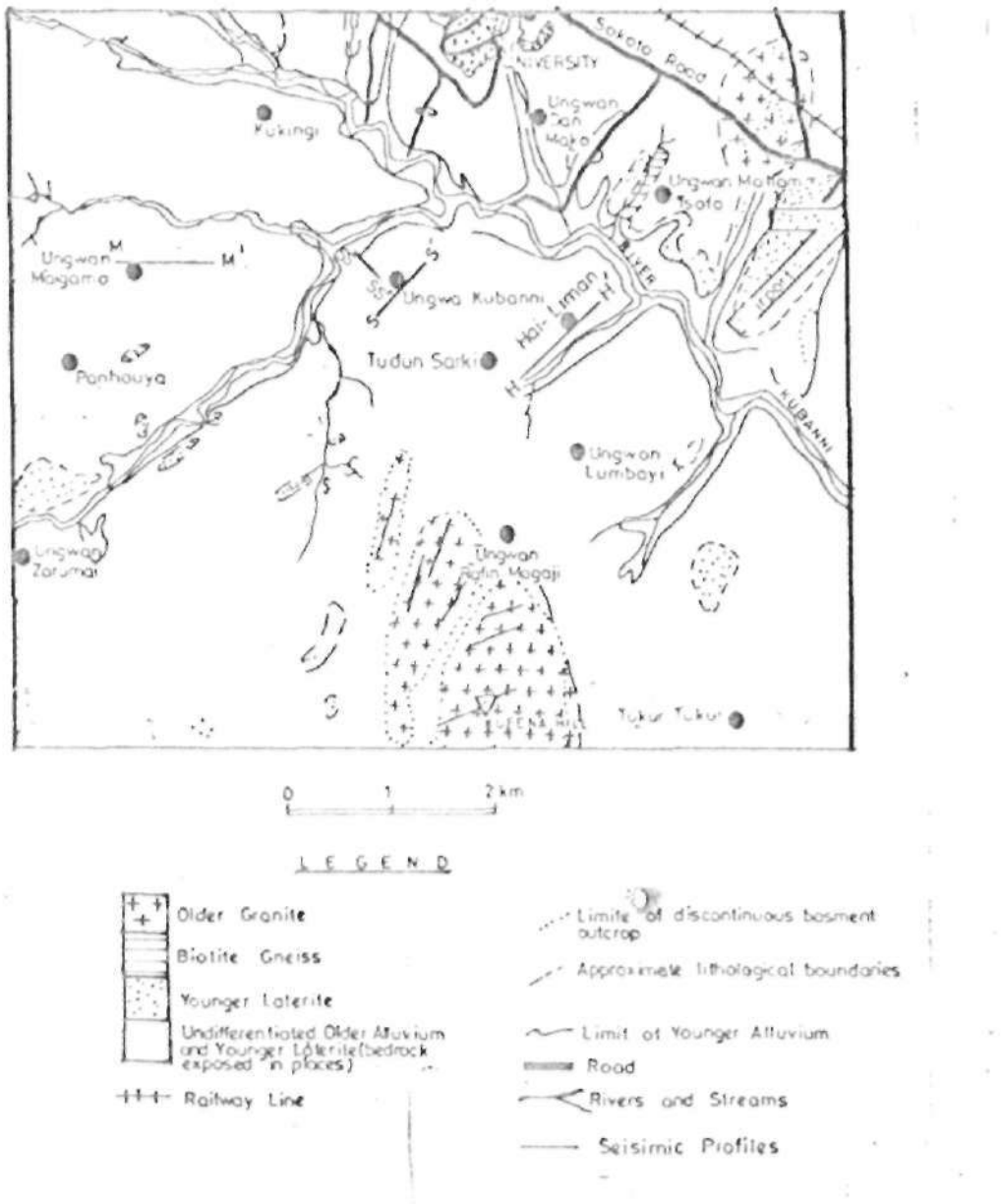


Fig.4.1: Part of the Kubanni Drainage Basin showing general layout of the seismic lines on the test field.

Also, inselbergs, whalebacks, granite pavements and isolated hills found within the project area are regarded as localized outcrops of the Zaria Batholith which belongs to the "Older granite" Complex (Eigbefo , 1978). The superficial deposits that cover most of the basement rock acts as recharge areas where they are underlain by weathered basement (Hassan,1987). These deposits are the Older Laterite and the Quarternary deposits which constitutes the sporadically distributed Older and Younger alluviums. Tokarski (1972) further classified the main components as Aeolian Cover, Upper Savannah Loam, Younger Laterite and Lower Savannah Loam.

4.3 Previous Studies in the Test Area

The investigations in the Kubanni Drainage Basin ranged from geological which include hydrogeology, geographical to geophysical. The major works of interest and their findings are summarised below in order of their importance to the present study.

4.3.1 Geophysical Work

Hassan (1987) carried out geo-electrical investigations in the area (See Figure 4.2) with the aim of determining subsurface layerings, locations and types of aquifers, basement geometry and favourable zones for siting water boreholes in the area. From the geo-electrical results, Hassan suggested the following:

(i) subsurface layering of 2 to 4;

(ii) undulating bedrock with depths generally increasing towards the southern part of the area (Fig. 4.2);

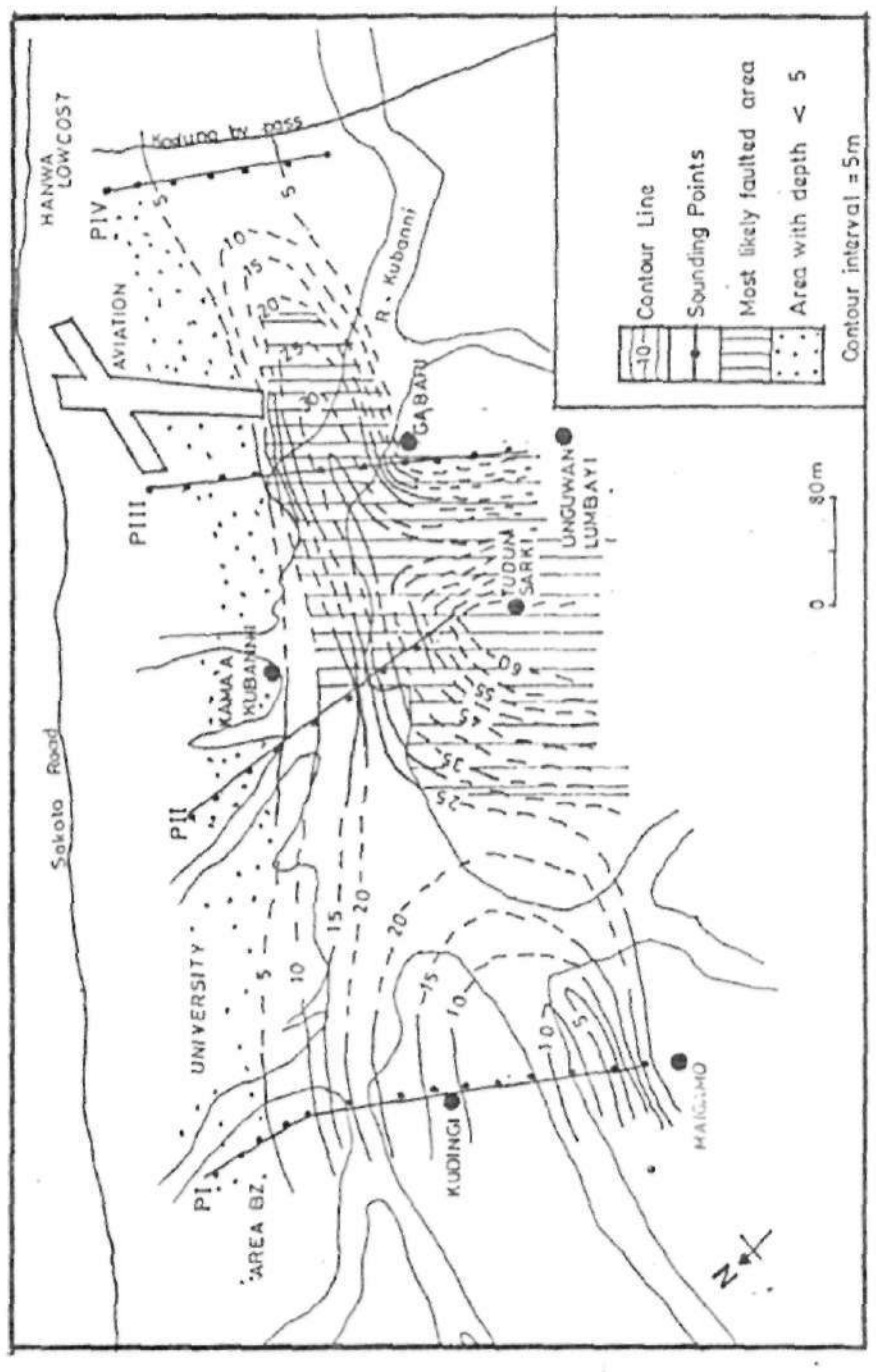


Fig. 4.2: Depth to basement map of the Kubanni Basin
(after Hassan, 1987)

(iii) a SE-NW and NE-SW trending depression in the area; and

(iv) weathered basement as the main aquifer in the area.

4.3.2 Geological Work

One of the most important geological works include that of Olowu (1967) who studied the surface water and its effects on the ground water in Zaria area. He found that wells dug away from the river have their water table falling progressively throughout the dry season. Also important were the works of McCurry (1970) and Wright and McCurry(1970). They carried out a study of the basement geology of Zaria Sheet No. 102 SW. They inferred from their work that the basement complex rock is made up of mostly Older granite and Biotite granite-gneiss. Eigbefo (1978) also studied the hydrogeology of the Kubanni Drainage Basin. He used hand-dug wells to establish that the depth to water table at various points in the area vary from 3 to 10m. He also emphasized the general dipping of the geologic layering in the direction of River Kubanni.

4.4 Data Collection:

4.4.1 Introduction

Since our primary interest here is the enhancement of low-quality seismic refraction data, the Kubanni Drainage Basin was particularly suited to this study for the following reasons:

(i) Previous investigations (Hassan,1987) had shown that the basement in the basin was relatively deep in some locations, being greater than 20m.

Therefore, in order to receive good refraction signals from the basement, a good energy source was required . However, only a low energy source was available.

(ii) The instrument used for the study was an ABEM TR10 12 - channel seismograph. Because of some logistics problems, explosives could not be used, and the signal source was the Mechanical Energy Source (MES). The result of this was that in deep basement areas, long spreads were needed and high amplifier gains required to pick the weak basement refractions. Consequently, signal-to-noise ratio was prone to be low.

(iii) There was a malfunction in the Signal Averaging System (SAS) of the seismograph which is designed to enhance weak signals by repeated addition of shots at the same location (Section 1.2.2), and this system could not be used.

Preliminary runs soon showed that spread length of more than 100m were required in most places to receive the basement refractions. It also became apparent that the instrument amplification required to receive them was such that the noise level was raised to a point where the signal quality became very low. It therefore appeared that ideal conditions for the use of the beam-forming technique had been found.

4.4.2 Instrumentation

The seismic equipment used consisted of a compact portable ABEM TR10 SX-12, Type 5352, seismograph. It is a 12 - channel, battery driven seismograph for ground investigation with the seismic refraction method, and measures

velocities by detecting ground vibrations produced by artificial energy source.

The main accessories include:

(i) an amplifier system which consisted of 12 solid state amplifiers; one for each channel,

(ii) recording system which consisted of lamps, galvanometers, optics, seismogram feed system and timing system,

(iii) 12 electrodynamic type seismometers with coil resistance which are sensitive to vertical velocity, and

(iv) the signal averaging system which could not be used due to a malfunction;

(v) shot system which consisted of a 10kg falling weight, impact plate, and falling weight guide tube equiped with weight-release and trigger (see instrument manual),

(vi) power supply, consisting of 24 rechargeable 1.25V nickel - cadmium cells in a tray,

(vii) shot transmission cable,

(viii) geophone cable, and

(ix) a geophone bag.

4.4.3 The Field Work:

The field work was conducted during seven days in May and June, 1989. The seismic refraction profiles covered a total distance of 1.54km comprising of four profiles with forward and reverse shootings carried out for each spread.

The general layout of the refraction lines are shown in Figure 4.1. The profile SS - SS' is located in Ungwa Kubanni Village in the NW-SE direction and is 220m long. The second profile S-S' in the same village was 330m long and trends in NE-SW direction. Other profiles include M-M' of length 440m trending E-W and located in Maigamo village, and H-H' profile of length 550m in NE-SW direction, and located in Hai-Liman village. Each of the profiles was segmented into refraction spreads of 110m each. Thus, the number of spreads in each profile varied from 2 in profile SS-SS' to five in profile H-H'. Each profile was selected to be parallel to the strike of the basement topography indicated by the depth -to-basement contours in Figure 4.2, except for profile SS-SS' which was a cross profile.

The profiling technique adopted involved laying 12 geophones with an inter-geophone spacing of 5 metres, and starting 5 metres from the shot point A, thus covering a total spread length of 60 metres (Fig. 4.3). After shot A which gives data for the first segment of the forward spread, the shot was shifted to the shot point B and repeated for the second segment of the reverse spread. The first nine geophones from shot point A were then shifted to the locations 13 to 21 leaving the last three as over-lapping geophones. The second reverse profile shot was made at the shot point B for the first segment of the reverse spread.

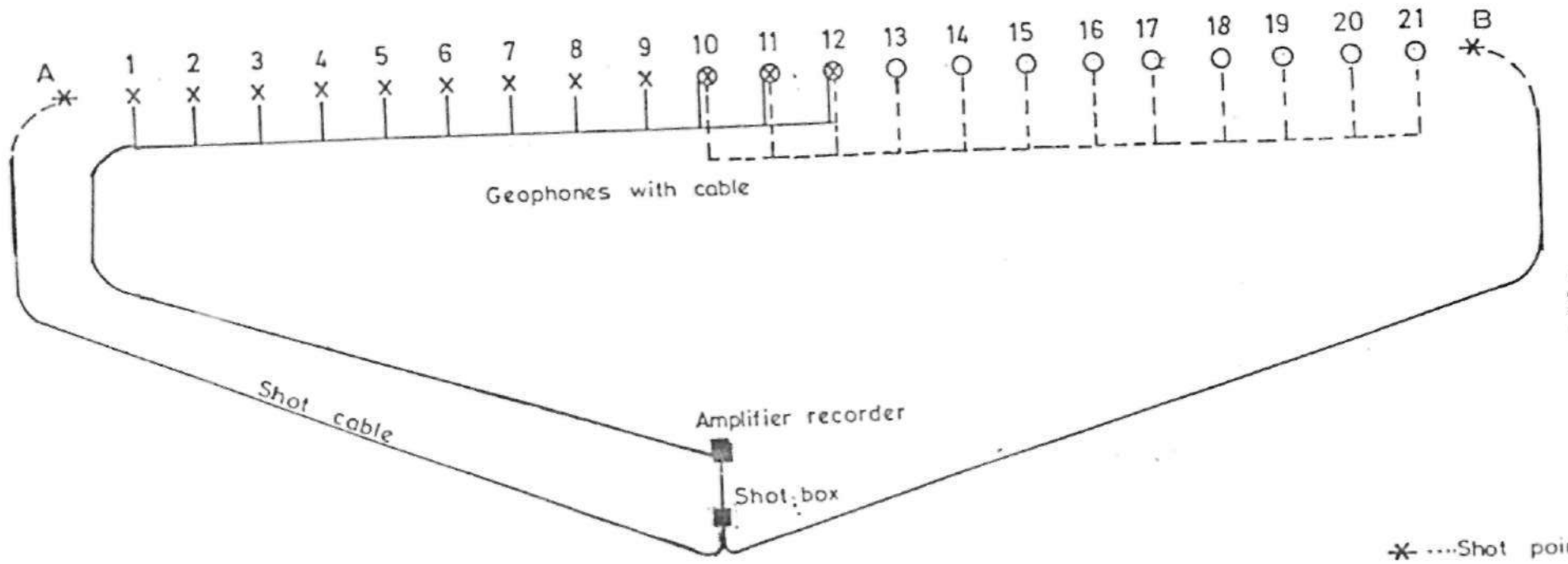


Fig. 4.3: The field set up indicating the profiling technique adopted

The shot was again repeated at pont A to complete the second segment of forward spread. All the geophones were then moved to another spread along the same profile and the same procedure repeated.

4.4.4 Problems Encountered

Later in the survey, there was a complete malfunction of the seismograph, and the work had to be prematurely terminated. This did not happen before ample data had been collected to verify the viability of the beam-forming technique. However, not enough data was collected for this part of the study to be considered a follow-up of the work of Hassan (1987).

4.5 Data Analysis and Interpretation:

The field data analysis was done in two stages:

(i) manual plotting of time-distance graph, and

(ii) use of the beam-forming computer programme.

The main essence of the first stage was to determine the preliminary velocities which would be used as steering velocities for the computer analysis, and to determine the top layer velocities needed by the programme for depth computations.

4.5.1 The Manual Time-Distance Plots

This involved picking the first arrivals from the low-quality field data. In general, variations in the quality of the seismic records obtained from the test profiles using the same shooting arrangement ranged from extremely noisy to moderately noisy ones.

Figures 4.4 and 4.5 show two examples of contrasting records. The difficulty involved in the manual picking of the first arrivals when the record quality is low can be seen from an inspection of Figure 4.4. On the other hand, the good quality record of Figure 4.5 shows clear trace-to-trace correlations and the onset of the refracted arrivals are very easy to pick. It is therefore for the former type of record quality (Fig. 4.4), which was common, that the beam-forming technique is particularly useful.

After picking the first arrivals from the seismograms, these were recorded against the corresponding geophone distances from the shot point for all the fourteen spreads that made up the four seismic lines shown in Figure 4.1. The values were then manually plotted (forward and reverse) and best-fit lines were determined for the various segments by visual inspection and drawn. Typical examples of such plots are shown for profile M-M' in Figure 4.6. The various layer velocities were obtained by taking the inverse of the slope of the individual line segments and the intercept times determined by extrapolating the second and the third velocity segments. Figures D.1, D.2 and D.3 (Appendix D) show the travel time plots for profiles S-S', SS-SS' and H-H' respectively.

4.5.2 Typical Interpretation of the Manual T-X Plots

It is not the aim of this study to interprete the manually plotted T-X graphs since these are only meant to serve as guide-lines to choice of ranges of steering velocities.

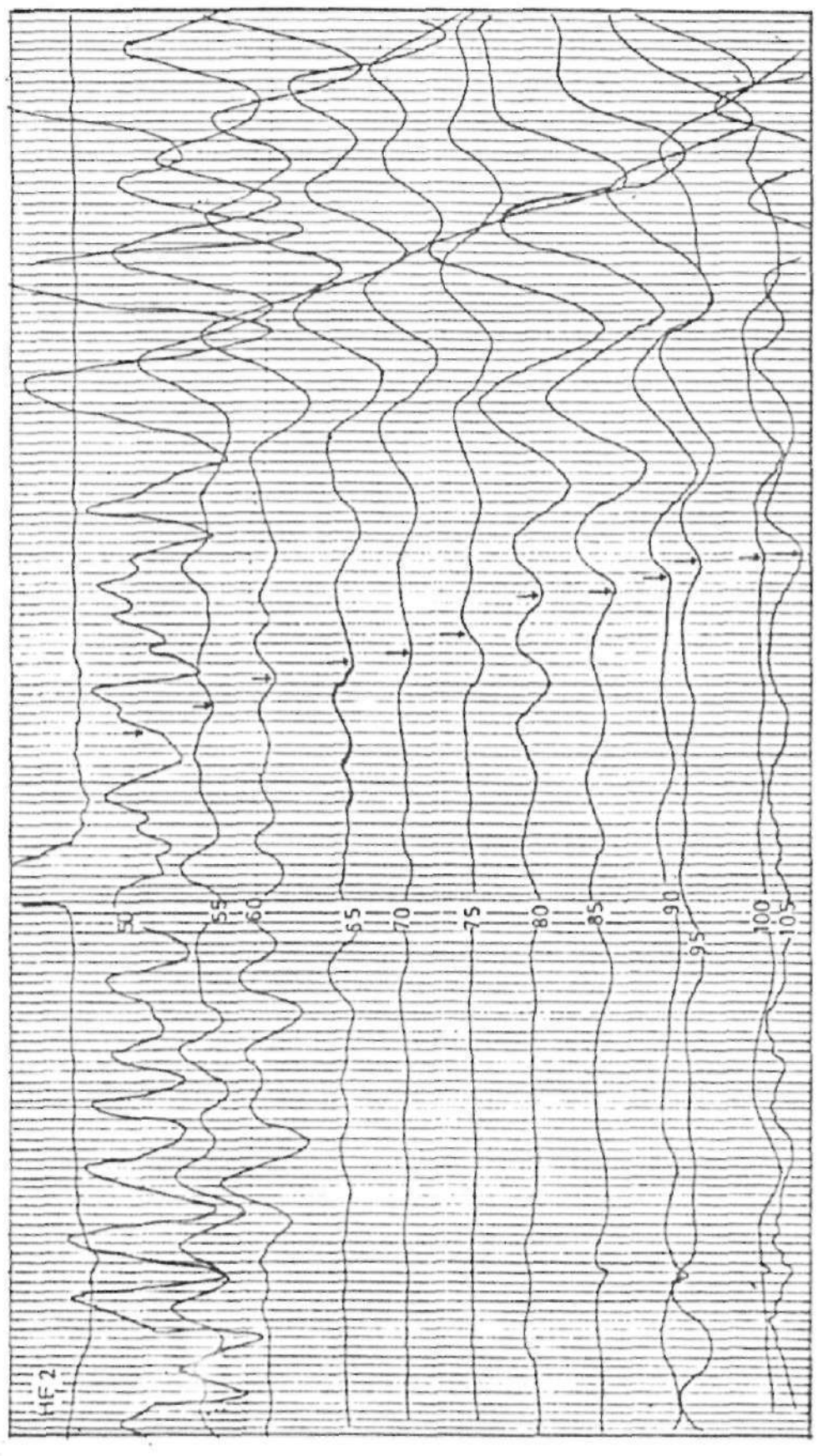


Fig. 4.4: A typical field record

The numbers 50 - 105 indicate geophone distances away from the shot point

The arrows show first arrivals picked.

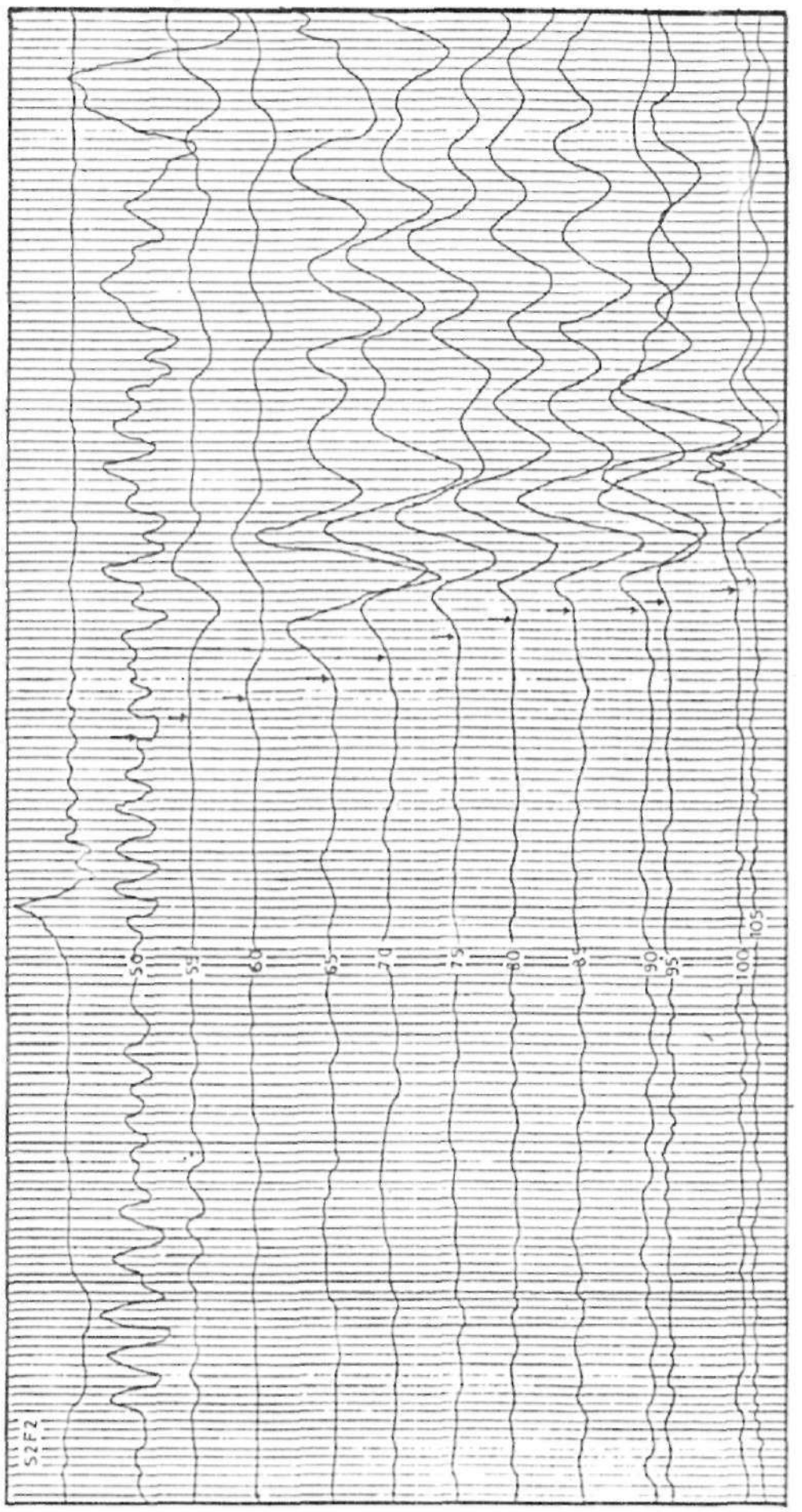


Fig. 4.5: A sample of a good quality field record (a rare case)
The numbers 50 - 105 are geophone distances away from the shot point
The arrows indicate first arrival times picked

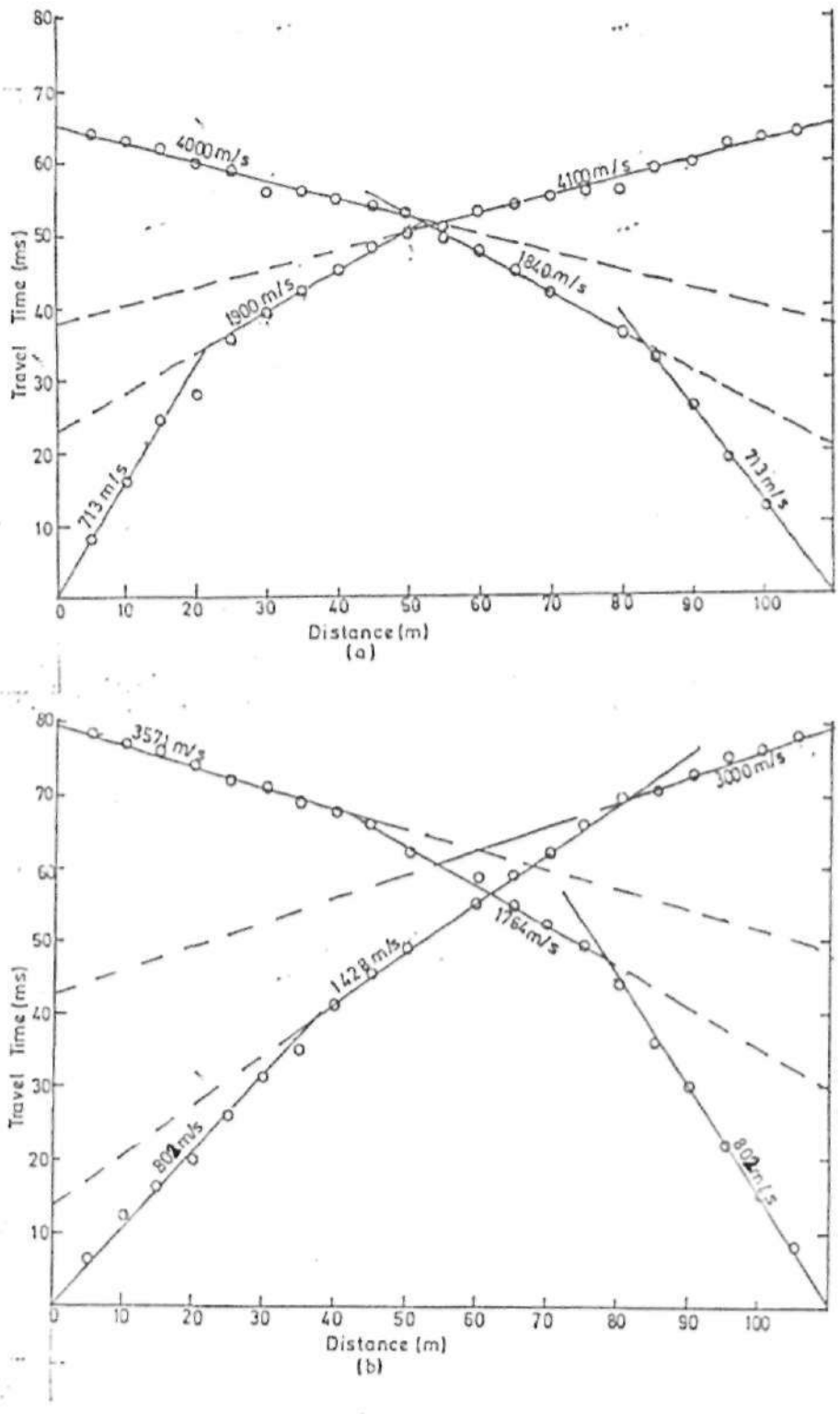


Fig. 4.6 (a) & (b): Manual T-X plots of the field data for spreads 1 & 2 of profile M-M'

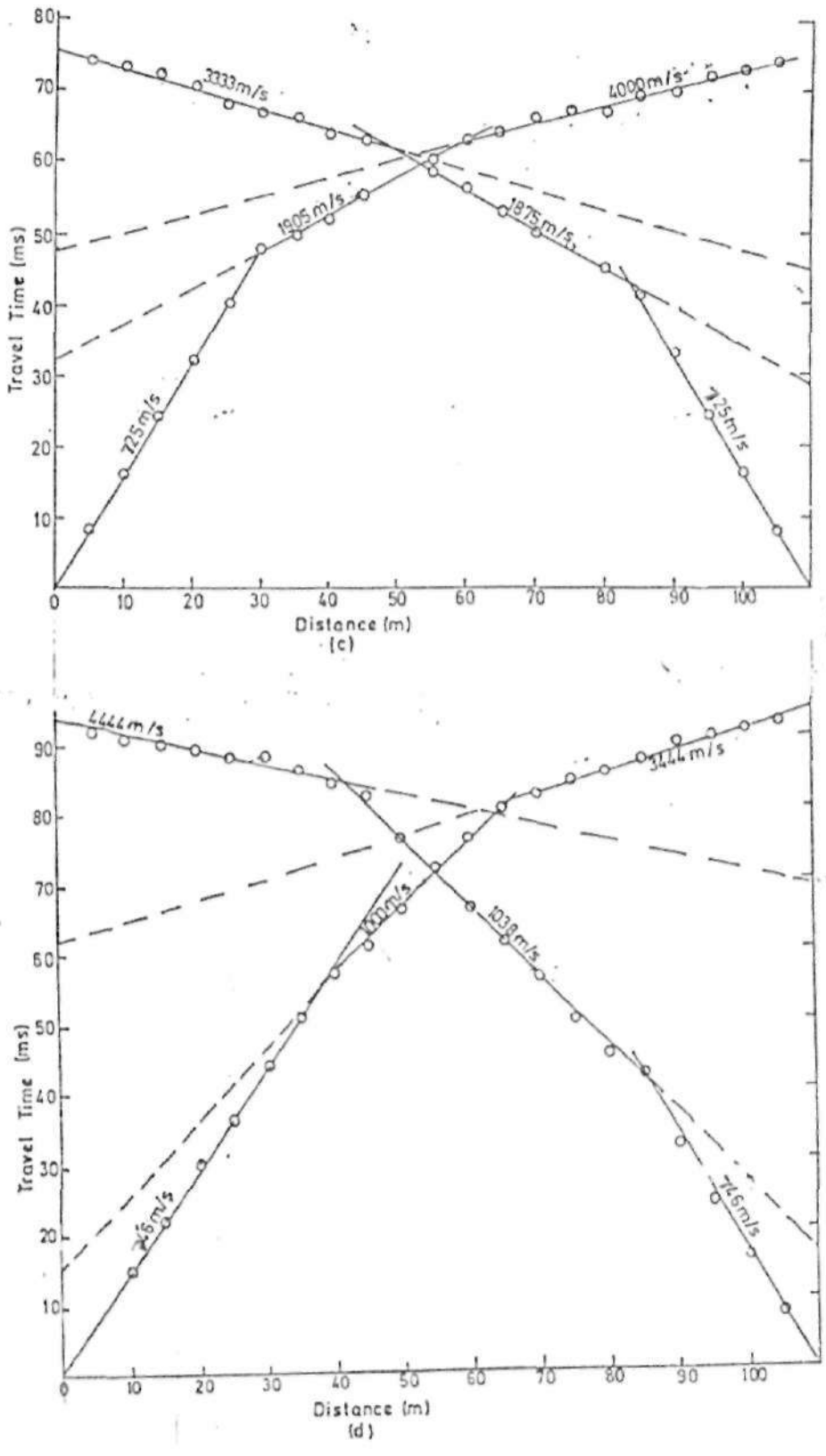


Fig. 4.6 (c) & (d): Manual T-X plots of the field data for spreads 3 & 4 of profile M-M'

Nevertheless, the typical T-X plots of Figure 4.6 are here interpreted to explain why the application of the beam-forming technique is preferred.

Velocity-depth section obtained for the manually plotted T-X graphs (Fig. 4.6) is shown in Figure 4.7. The section shows three geologic layers with thickness of the first layer varying between about 7m and 12m while that of the second layer ranges from about 14m to about 22m. The section also suggests varying depth-to-basement of about 25m in some places to more than 30m in other places. It is obvious from the section that the basement surface generally dips away from the River Kubanni which is in the eastern side of Figure 4.7. Also obvious is the inconsistency in the direction of dip from spread-to-spread suggested by the section.

As earlier emphasized, some of these results may be unreliable, being acquired from seismic records in which the first arrival times were not very clear (Fig. 4.4). Nevertheless, to assess the closeness of these results with those of the beam-forming technique and the previous works in the same location, correlations between the deductions from the section and those of the beam-forming computer programme, and the previous investigations in the same area are discussed later (section 4.6).

4.5.3 Application of the Beam-Forming Technique

A continuous seismic trace may be converted into a sequence of numbers. Each number thus represents the amplitude of the trace at a specified time instance

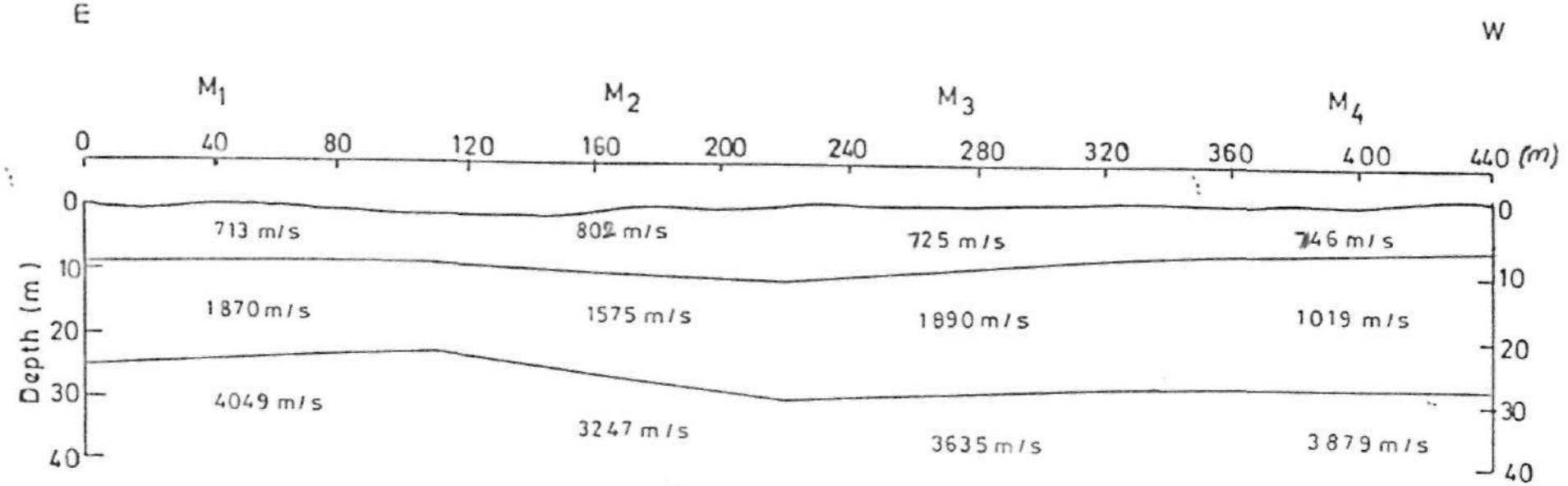


Fig. 4.7: Manual Velocity/Depth Section for profile M-M'. M_1 to M_4 indicate geophone spreads

(Anderson & McMechan, 1988; Cassano & Rocca, 1973 and White, 1977). The time points are chosen to be equally spaced so that the time interval between two consecutive readings of the trace is always the same. The process of converting a continuous trace into a sequence of numbers of equally spaced time points is called digitization.

Since digital computer was to be used for the analysis, digitization of the traces on the field records formed an important aspect of this method of analysis. Factors such as trough-to-trough or crest-to-crest correlation of the traces, the possible onset times of the signals and the frequency characteristics of the signals were taken into consideration in the attempt to obtain a digital representation of the analogue signals. The highest frequency component of the seismic traces on the field records was then estimated to be about 125 HZ. Since distortion of the output frequency (aliasing) could be avoided by choosing a sampling rate (SR) greater than twice the highest-frequency component of the signal (Kanasewich, 1975; Dobrin, 1976), a digitizing interval of 1ms corresponding to a SR of 1 KHZ was used. A window length of 60 ms was also selected for all the traces to be digitized. Horizontal, zero-amplitude lines were then drawn through the centre of the individual traces. Although the onset times of the refractions were not often obvious, their locations on most of the traces could be estimated. With this estimate, digitization was started a few milliseconds before the onset of the signals.

Using the trace-to-trace correlation of the records collected for each spread and guidance from the manual T-X plots, the digitized traces were grouped into second-layer and third-layer segments. These and the distances of the traces from shot point, the estimated on-set times of the signals, the number of traces per segment, number of points digitized, number of points used to from the beam, initial sweep velocity, the final sweep velocity, the digitizing interval and the sweep velocity increment form the input data of the computer programme (See Appendix A). The ranges of the sweep velocities for the second and third layers were estimated from the manual T-X plots. The output of the computer programme consisted of apparent layer velocities and the corresponding intercept times, the actual layer velocities, thicknesses of the various layers and the dips of the geologic interfaces. Table 4.1 is a typical computer output of the field result. It contains both the input and output parameters mentioned above. The "TM inter" refers to intercept time while H_u and H_d indicate depths under up-dip and down-dip shot points respectively.

4.5.4 Interpreting the Results of the Beam-Forming Computer Programme

As earlier stated, the field data described here were not intended for a detailed analysis of the Kubanni Drainage Basin but rather to serve in verifying the efficacy of the beam-forming technique. Because of the limited number of the seismic refraction profiles involved, it will not be possible to give a detailed interpretation of the basement structure of the basin.

Table 4.1: A typical computer output of the field result.

HAI-LIMAN, SPREAD 5, FORWARD PROFILE, 2ND LAYER

NO OF TRACES= 5 NO OF POINTS/BEAM= 100 N O OF POINTS IN TRACE= 60
SAMPL.INT.= 1.0 VSTRT,VSTOP= 1000.0 1800.0 VEL INCREMENT= 10.0

CHANNEL	DISTANCE	START TIME
1	30.0	36.0
2	35.0	38.0
3	40.0	39.0
4	45.0	41.0
5	50.0	42.0

2ND LAYER (F.PROF)VEL=1300.0 TM INTER.= 13.00

HAI-LIMAN, SPREAD 5, REVERSE PROFILE, 2ND LAYER

NO OF TRACES= 4 NO OF POINTS/BEAM= 100 N O OF POINTS IN TRACE= 60
SAMPL.INT.= 1.0 VSTRT,VSTOP= 700.0 1400.0 VEL INCREMENT= 10.0

CHANNEL	DISTANCE	START TIME
1	30.0	43.0
2	35.0	45.0
3	40.0	48.0
4	45.0	51.0

2ND LAYER(R.PROF)VEL= 760.0 TM INTER. = 9.00

HAI-LIMAN, SPREAD 5, FORWARD PROFILE, 3RD LAYER

NO OF TRACES= 7 NO OF POINTS/BEAM= 100 N O OF POINTS IN TRACE= 60
SAMPL.INT.= 1.0 VSTRT,VSTOP= 2700.0 3500.0 VEL INCREMENT= 10.0

CHANNEL	DISTANCE	START TIME
1	75.0	59.0
2	80.0	60.0
3	85.0	61.0
4	90.0	63.0
5	95.0	63.0
6	100.0	65.0
7	105.0	65.0

3RD LAYER(F.PROF)VEL=3460.0 TM INTER = 38.00

HAI-LIMAN, SPREAD 5, REVERSE PROFILE, 3RD LAYER

NO OF TRACES= 5 NO OF POINTS/BEAM= 100 NO OF POINTS IN TRACE= 60
SAMPL.INT.= 1.0 VSTRT,VSTOP= 2000.0 2800.0 VEL INCREMENT= 10.0

CHANNEL	DISTANCE	START TIME
1	75.0	58.0
2	80.0	58.0
3	85.0	61.0
4	90.0	64.0
5	95.0	64.0

3RD LAYER (R.PROF) VEL= 2010.0 TM INTER = 24.00

Table 4.1: (Cont'd)

V1 = 600.0

V2= 937.1	V3=2531.7
H1U = 5.08	H2U =10.88
H1D = 3.51	H2D = 8.37
DIP1D = .69	DIP2D = 5.60

The end results of the application of the beam-forming technique to real data are the geologic sections of Fig. 4.8 to 4.11. The sections were obtained using published P-wave velocity ranges for various rock units (Mooney, 1973; and Nkuesenam, 1976), velocities and depths obtained from the beam-forming Computer Programme of Appendix A. The lengths of each profile and the corresponding thicknesses of its layers have been drawn to scale.

The sections display four important characteristics of the geologic layerings of some parts of the Kubanni Drainage Basin. These are:

(i) the number of layers and the estimated thicknesses of the various geologic layers;

(ii) the general direction of dips of the geologic layering in the part of the basin covered;

(iii) estimated depths to basement, and

(iv) interpreted geologic units.

The velocity/depth sections (Fig. 4.8 to 4.11) show different geologic layering thicknesses ranging from about 4m to 14m. These thicknesses are comparable with those deduced by Eigbefo (1978), who found out that the thicknesses of the layers were irregular, varying fr m less than 5m to as much as 15.2m in some places. The sections also suggest 3 geologic layers along the refraction lines.

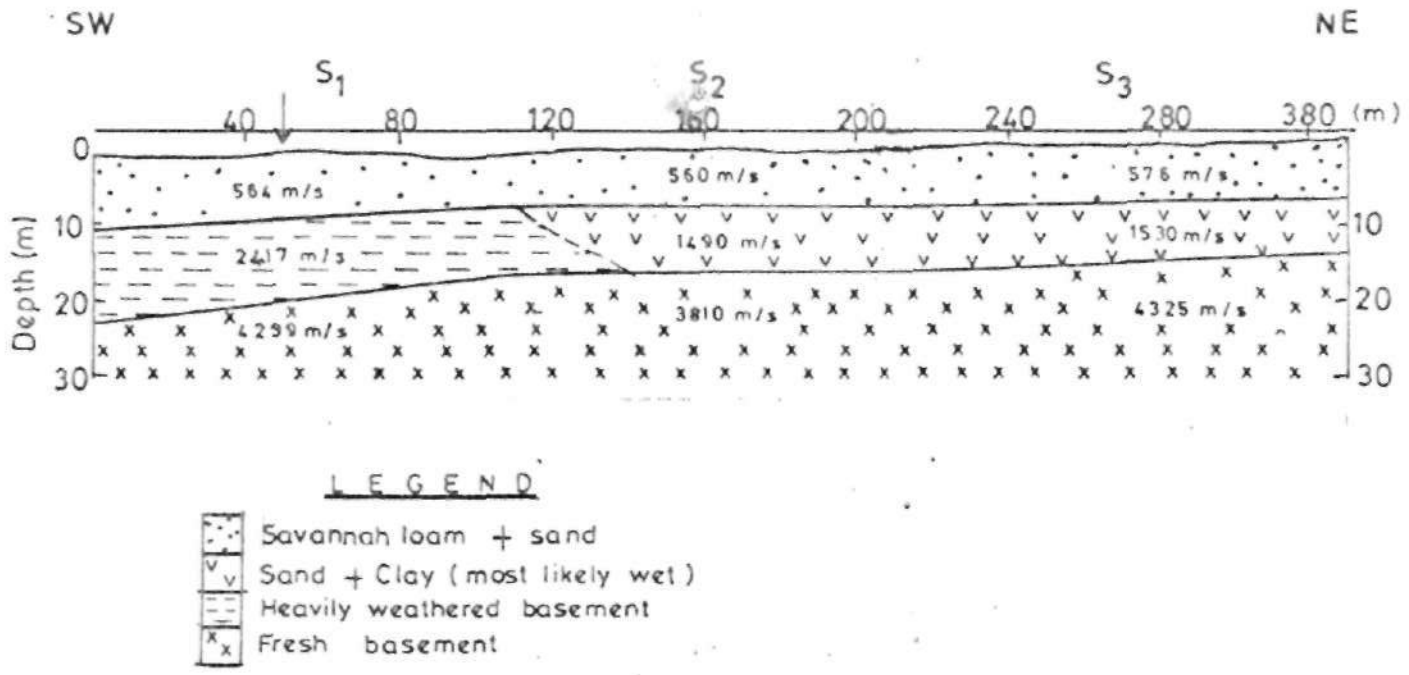


Fig. 4.8: Geologic Section for Profile S - S'
S_1 to S_3 indicate geophone spreads
Arrow shows well location
SW South - West
NE North - East

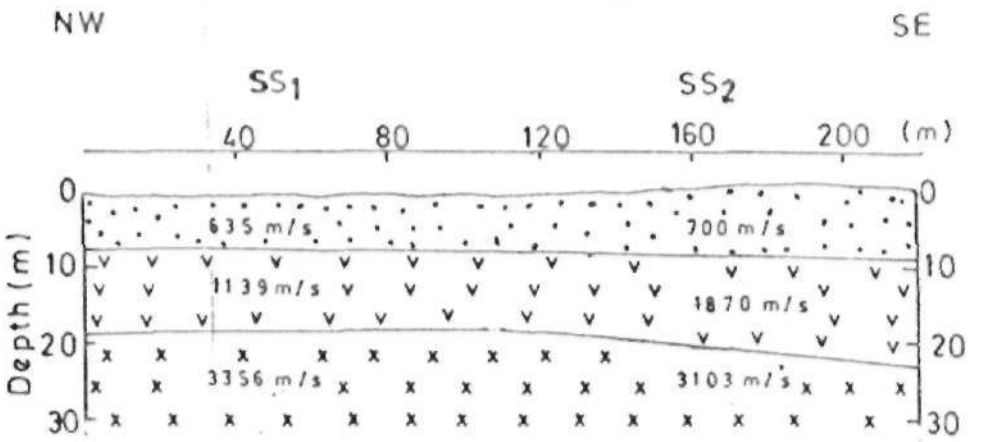


Fig. 4-9 : Geologic Section for profile SS - SS'
SS_1 & SS_2 indicate geophone spreads
NW North - West
SE South - East

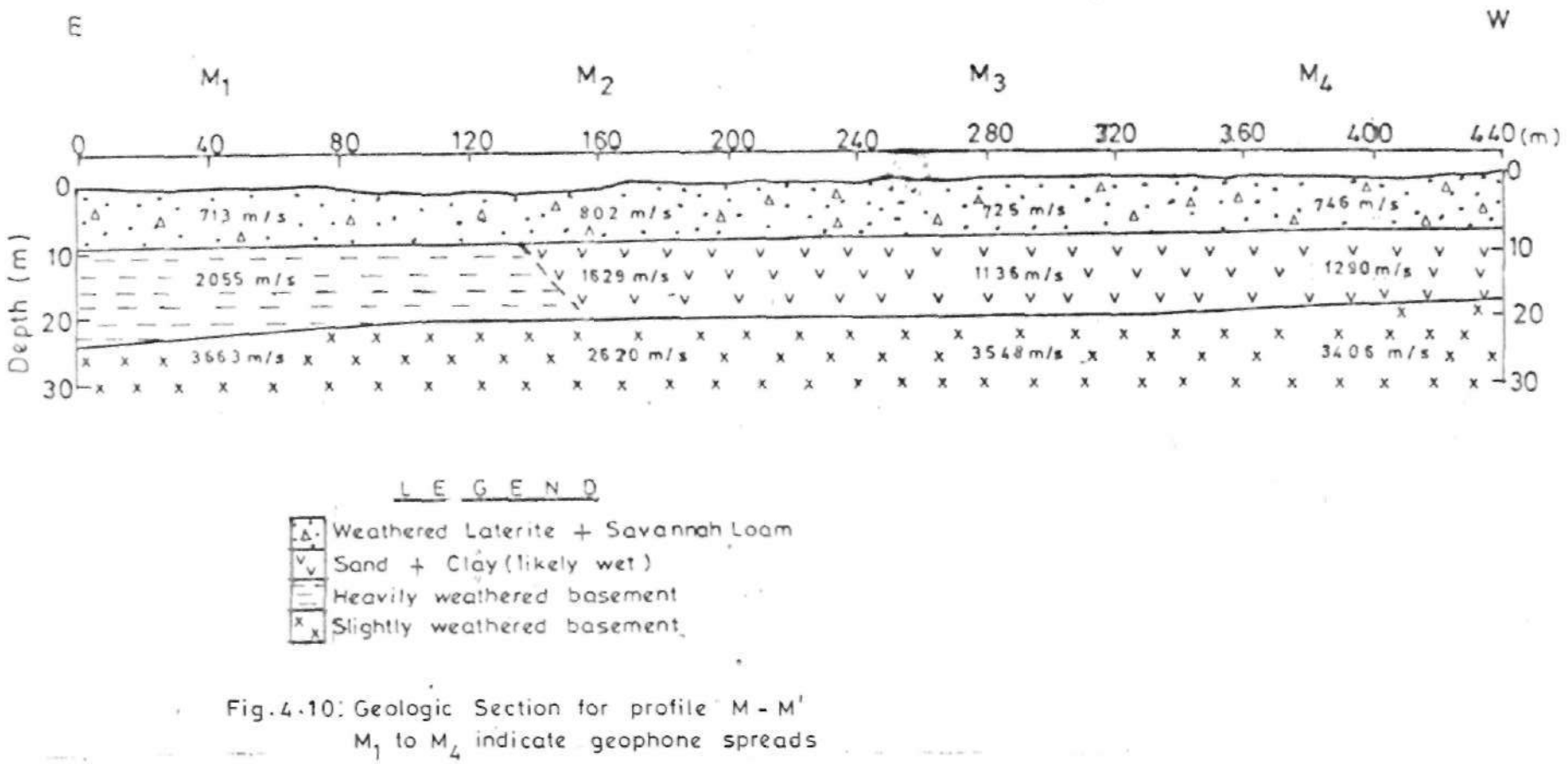


Fig. 4.10: Geologic Section for profile M - M'
M_1 to M_4 indicate geophone spreads

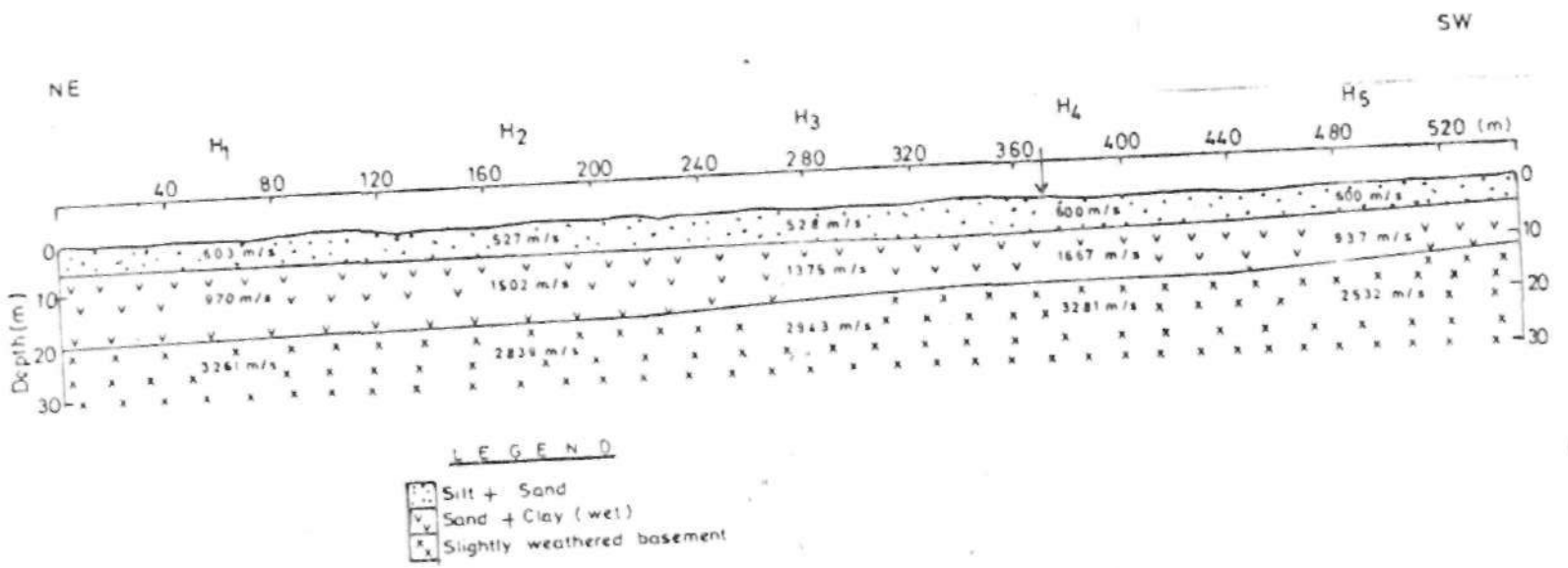


Fig. 4.11: Geologic Section for profile H - H'
H_1 to H_5 indicate geophone spreads
Arrow indicates well site
NE North - East
SW South - West

These results agree with those obtained by Hassan (1987) at the same locations; for instance, Maigamo village.

The sections of Figures 4.10 and 4.11 were derived for the seismic refraction lines M-M' and H-H' respectively (Fig. 4.1). It is obvious from the two figures that the geologic layers at these locations dip generally in the direction of River Kubanni to the east of Figure 4.10 and to the north-east of Figure 4.11. These suggested dip directions are in agreement with the findings of earlier workers such as Olowu (1967) and Eigbefo (1978), who stated that the geologic layerings in the basin generally dip in the direction of the River Kubanni. On the other hand, the geologic sections obtained for profiles S-S' and SS-SS', both located around Ungwan Kubanni, suggest dipping of the geologic layerings away from the River Kubanni. Since the two profiles are perpendicular to each other, these results probably suggest a depression with the deepest part towards the southern part of Ungwan Kubanni (Fig. 4.1). This suggestion is in agreement with that of Hassan (1987) who suggested the existence of relatively deep depression (upto 60m deep) in that part of the Kubanni basin.

The geologic sections of Figure 4.8 and 4.10 suggest depth-to-basement of 16m to 25m, and about 20m to 24m around the Ungwan Kubanni and Maigamo villages respectively. The section in Figure 4.11, obtained for profile H-H', also suggests basement depths ranging from about 12m to 20m at the Hai-Liman village.

These suggestions closely agree with those of Hassan (1987) who deduced basement depth of about 25m, 25m to 30m and 15 to 25m for Ungwan Kubanni, Maigamo and Hai-Liman villages respectively.

The geologic units in the velocity/depth sections of Figures 4.8 to 4.11 have been obtained on the basis of P-wave velocity ranges for different rock types (Mooney, 1977; Ntaji, 1979) and the geology of the area (McCury, 1970). The assumed geologic units adequately agree with those of Hassan (1987) for resistivity profiles close to the seismic profiles concerned.

Depth to water level in hand-dug wells indicated on S_1 (Fig. 4.8) and H_4 (Fig. 4.11) were measured to be about 11.1m and 7.3m respectively during the field work. These depths correspond to subsurface layering with P-wave Velocities of 2417m/s and 1667m/s respectively. The difference in the velocities at the two locations is most probably associated with the different aquifers suggested by Olowu (1967) and Eigbefo (1978) and confirmed by Hassan (1987), that the aquifers in the Kubanni Drainage Basin were basically weathered basement, alluvial deposits (sand + clay) and older Laterite. Since non of the geo-electrical profiles (Hassan, 1987) passed through these two locations, the type of aquifers at well locations can only be inferred from P-wave velocity ranges. Therefore, comparing velocity ranges of 610 - 1830m/s and 915 - 2750 m/s for wet sand and wet clay respectively, and 3050 - 5490m/s for fresh gneisses (Mooney, 1977; Nkuesenem, 1976), it may be reasonable to assume weathered basement as the aquifer at the well site located on the geophone spread S_1 (Fig. 4.8) and sandy clay as the aquifer at geophone spread H_4 (Fig. 4.11). Using this well correlation and field observation of a relatively far away well in the Maigamo village, a subsurface layer with P-wave velocity of 1629m/s at a depth of about 9m is

most probably a relatively thick sandy clay aquifer, located on geophone spread M_2 of profile M-M' (Fig. 4.10) to the North of the village.

4.6 Comparing Typical Manual Results with those of Beam-Forming Technique:

To assess the relative reliabilities of the results of the beam-forming technique and those of the manual method, another set of results obtained in the same area is needed for comparison. For this reason, profile M-M' has been manually interpreted (Secion 4.5.2), being the only profile that is adequately close to the geo-electrical line P_I(Fig.4.2) laid by Hassan (1987) for meaningful correlations.

The velocity/depth section obtained manually is displayed together with that of the beam-forming technique along the same profile (Fig. 4.12). The general dipping of the basement surface away from the Kubanni river suggested by the section (Fig. 4.12 (a)) obtained from the manual T-X plot does not agree with the deduction from the geo-electrical results by Hassan (1987) that the layers dip in the direction of River Kubanni. On the other hand, the beam-forming section(Fig.4,12(b)) is in agreement with the deduction of the geo-electrical work. The inconsistency in the direction of dip shown by the manual section reveals the inaccuracy in the picking of the first arrival times caused by the low-quality of the data. On the other hand, the depths to basement of as much as 32m and 25m suggested by Figure 4.12(a) and 4.12 (b) respectively adequately agree with the range of 25m to 30m suggested by Hassan(1987).

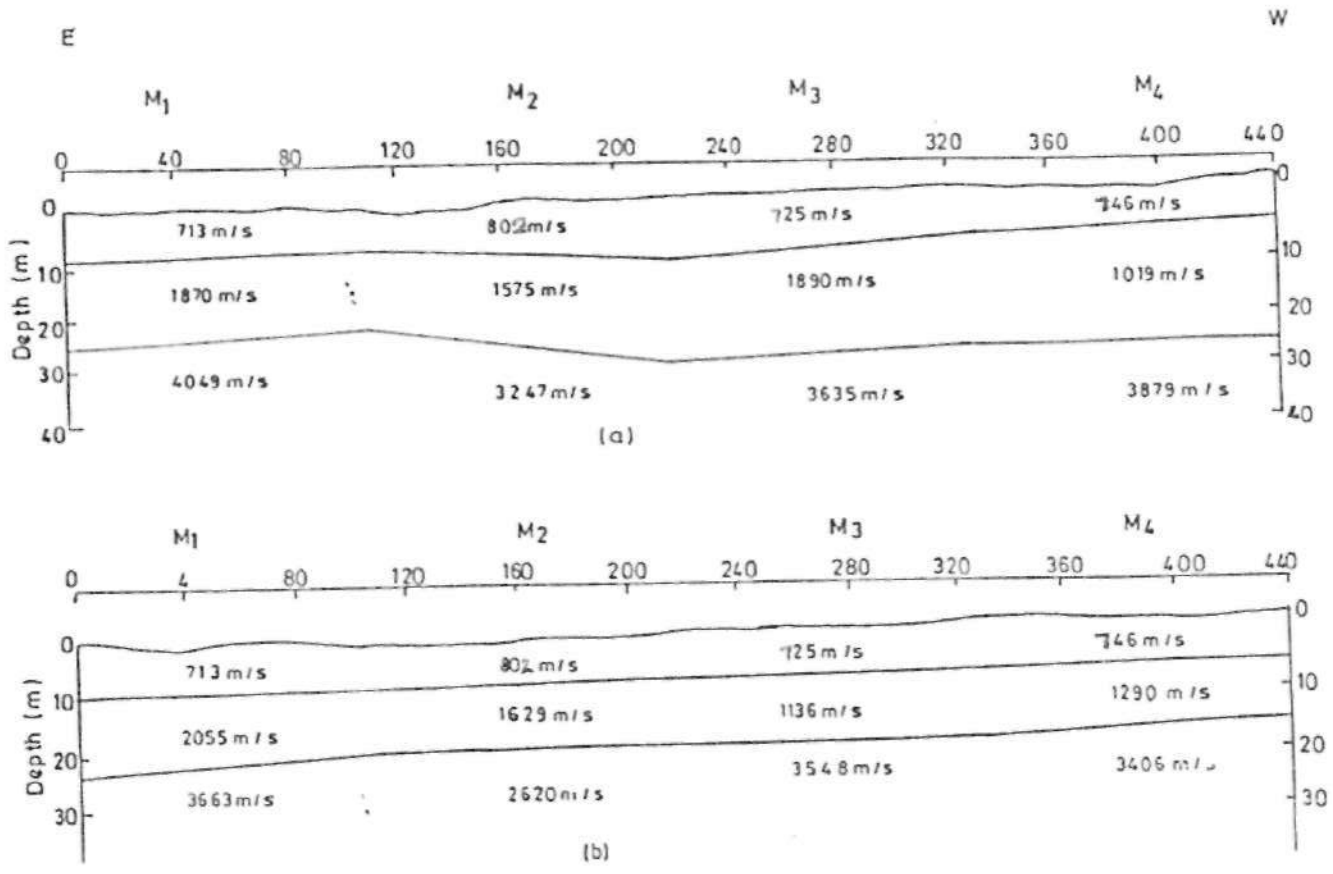


Fig. 4.12: Comparison between manual and computer determined sections

(a) Manual section

(b) Beam-forming section

The layer velocities of both sections are adequately correlated.

It is therefore obvious from the above comparisons that the beam-forming technique gives more reliable results of a low-quality seismic refraction data than the manual method. Nevertheless, it is also obvious that the results of the beam-forming technique fairly agree with those of the manual method even when the two are used to analyse poor quality data.

CHAPTER V

DISCUSSIONS, RECOMMENDATIONS AND CONCLUSIONS

5.1 Limitations of Beam-Forming Technique and Suggestions for Further Work:

The seismic traces combined to form the beam signal were grouped on the basis of the outcome of the manual T-X plots and the observed trace-to-trace correlations. However, the end traces of a given velocity segment may some times not all correspond to the same refractor. The trace-to-trace correlations were in some cases made very difficult by the nature of the noise involved. These two factors may lead to wrong combination of seismic traces for a given refractor. The end result of this is a distorted beam that does not correspond to the correct seismic wave velocity for the layer. This could be the cause of some unexpected changes in the layer velocities in some sections of Figures 4.8 to 4.11. In search of a solution to the above problem, further studies are here recommended on how the beam-forming technique could be used to automatically determine the group of seismic traces that should belong to the same refractor by examining some properties of the individual traces.

The beam-forming technique can not give an appreciable improvement in signal-to-noise ratio of a low quality data containing mostly coherent noise. It cancels out only random part of the noise so that the beam formed may contain coherent noise before the on-set of the beam signal.

This may constitute a serious limitation of the beam-forming technique. For instance, the intercept time for a particular refraction branch was determined on the basis of the statistical estimation of the highest frequency component of the seismic signals shown on the traces (Section 2.2.1). This method was found to be very accurate in the absence of coherent noise on the formed beam. On the other hand, if the noise before the on-set of the signal is coherent, an intercept time far smaller than the correct value may be picked by the computer programme. It is therefore recommended that: (i) a better technique that does not depend upon the statistical estimation used here, be designed for determining accurate intercept times in the application of the beam-forming technique. (ii) the low quality record containing greater amount of coherent noise than random noise be analysed using an alternative method explained by Dobrin (1976) for attenuating coherent noise.

The manual digitization of the seismic traces is not only tedious, but may also be errorneous if adequate precautions are not taken in the choice of 'zero-amplitude line' and in recording the discrete amplitudes of the traces. The manual method might have introduced some errors in the results obtained. It is therefore suggested that the actual accuracy of the beam-forming technique be tested in different noise environments using a digital recording system in recording the seismic traces.

5.2 Conclusions:

If an appreciable improvement in signal-to-noise ratio is to be achieved when using low sources of seismic energy in a relatively noisy environment without the use of signal enhancement systems, some form of processing is essential. In this study, some causes of seismic noise and the capabilities of various types of field techniques and digital processing methods have been reviewed. This was an attempt to assess the level of signal-to-noise ratio improvements so far achieved with the known methods, and how these improvements correlate with that attainable using the beam-forming technique.

The automatic procedure for the processing of low-quality seismic refraction data presented in this work include automatic determination of layer velocities and the corresponding intercept times which are used to compute other layer parameters. A computer programme based on this procedure has been written and tested on a large amount of data including noiseless and noisy synthetic data and real data collected from the Kubanni Drainage Basin. It was found to perform excellently with an accuracy of upto 95% on noiseless synthetic data and better than 80% on noisy synthetic data. The beam-forming technique was also considered to have performed reasonably well with the real data based on the fact that it has been able to confirm some of the deductions such as the number of layers, the direction of dips of the geologic layering and the approximate depth to basement, of the earlier geologic and geo-electrical investigations in the Kubanni Drainage Basin.

This has therefore demonstrated that the beam-forming technique represent a powerful and viable method of extracting useful information from low-quality seismic refraction records.

References

1. Anderson, R.G. and McMechan, G.A., (1988): Noise-Adaptive filtering of seismic shot records, Geophysics vol. 53, No. 5, pp. 638 - 649.

2. Cassano, E. and Rocca, F., (1973): Multichannel linear filters for optimal rejection of multiple reflection, Geophysics Vol. 38, pp. 1053 - 1061.

3. Denham, D., (1963): The use of geophone groups to improve the signal-to-noise ratio of the first arrival in refraction shooting, Geophysical prospecting vol. 11, No. 4, pp. 389.

4. Dobrin, M.B., (1976): Introduction to Geophysical Prospecting, McGraw-Hill Book Co. New York.

5. Dobrin, M.B.; Lawrence, P.L. and Sengbush, R.L., (1954): Surface and near surface waves in the Delaware Basin, Geophysics Vol. 19, pp. 675 - 715.

6. Eigbefo, C., (1978): Hydrogeology of the Kubanni Drainage Basin, Zaria. unpublished M.Sc. Thesis, A.B.U., Zaria.

7. Ervin, P.C.; McGinnis, L.D.; Otis, R.M. and Hall, K.C., (1989): Automated analysis of marine refraction data, a computer algorithm, Geophysics Vol. 48, No. 5, pp. 582.

8. Gelchinsky, B. and Shitivelman, V., (1983): Automated picking of first arrivals and parameterization of travel time curves, Geophysical prospecting Vol. 31, No. 6. pp. 915 - 928.

9. Hassan, M., (1987): Geo-electrical investigations of the western half of the Kubanni River Basin, Zaria Nigeria, Unpublished M.Sc. Thesis, A.B.U., Zaria.

10. Howell, L.G.; Neuenchwander, E.F. and Pierson III, A.L., (1953): Gulf coarst surface waves, Geophysics vol. 18, pp. 41 - 53.

11. Kanasewich, E.R., (1975): Time sequence analysis in Geophysics, University of Alberta Press.

12. Mayne, W.H., (1962): Common reflection point horizontal stacking techniques, Geophysics vol. 27, pp. 952 - 965.

13. McCurry, P., (1970): The geology of the degree sheet 21, Zaria, Unpublished M.Sc. Thesis, A.B.U., Zaria.

14. Merchant, M.J., (1979): The ABC's of Fortran Programming, Wadsworth publishing Co., California.

15. Mooney, H.M. (1977): Hand-book of Engineering Geophysics, Minnesota, Biston Instrument, Inc.

16. Nkuesenam, O.E., (1976): Investigation of the extent of Kaolin Deposit near Tsanyawa, Kano State, Nigeria, Using Geo-electrical and seismic refraction methods, M.Sc. Thesis, A.B.U., Zaria.

17. Ntaji, F.A. (1979): Resistivity and seismic refraction methods for ground water exploration in malumfashi, Kaduna State, Nigeria. Unpublished M.Sc. Thesis, A.B.U., Zaria.

18. Ojo, S.B. and Mereu, R.F., (1983): Regional difference in upper mantle heterogeneity from coherent measurements on array data. Geophysical Journal of the Royal Astronomical Society, Vol. 72, pp. 173 - 192.

19. Olowu, J., (1967): Preliminary investigations of the groundwater conditions in Zaria sheet 102 SW, GSN report No. 1462.

20. Redpath, B.B., (1973): Seismic Refraction Exploration for Engineering Site Investigations. Distributed by National Technical Information Service, U.S. Department of Commerce.

21. Singh, S., (1978): An interactive method for detailed depth determination from refraction data for an uneven interface, Geophysical Prospecting Vol. 26, No., 2, pp. 3030.

22. Telford, W.M.; Geldart, L.P.; Sheriff, R.E. and Keys, D.A., (1976): Applied Geophysics, Cambridge University Press.

23. Tokarski, A., (1972): Hetrogenous terrace arrangement west of A.B.U., Ocassional Paper No. 2. Department of Geology, A.B.U., Zaria.

24. White, R.E., (1977): The performance of the optimum Stacking filters in suppressing uncorrelated noise. Geophysical Prospecting, Vol. 25, pp. 165 - 178.

25. Wright, J.B. and McCurry, P., (1970): Geological Map of the Zaria Area Sheet 102 - Zaria and its region, Mortimore (ed) occasional paper No. 4, Department of Geology, A.B.U., Zaria.

A P P E N D I X 'A'

BEAM-FORMING COMPUTER PROGRAMME

```
      PROGRAM ARRAY
C
C     PROGRAM STEERS REFRACTION SPREAD TO EHAHNCE WEAK REFRACTIONS
C     USES TRIAL VELOCITIES TO FORM BEAM. INSTANTANEOUS BEAM ENERGY
C     IS MAXIMUM WHEN STEERING VELOCITY EQUALS REFRACTION VELOCITY.
C
C     INPUT:
C           NCH         NO OF TRACES TO BE USED
C           NPT         NO OF POINTS USED TO FORM BEAM
C           NTRACE      NO OF POINTS DIGITIZED
C           DT          DIGITIZING INTERVAL
C           VSTRT       INITIAL TRIAL VELOCITY
C           VSTOP       FINAL TRIAL VELOCITY
C           DV          VELOCITY INCREMENT FOR ANALYSIS
C           X(I)        DISTANCE OF ITH TRACE FROM SHOT POINT
C           TSTRT(I)    TIME OF FIRST NON_ZERO AMPLITUDE ON I-TH TRACE
C           CHA(I)      DIGITIZED VALUES FOR I-TH TRACE
C     OUTPUT:
C           STEERING VELOCITY AND CORRESPONDING BEAM ENERGY
C
      DIMENSION TIT(20), X(12), TSTRT(12), CHA(12,200)
      OPEN (UNIT =6,FILE='OUT2')
C
C     READ IN DATA COMMON TO BOTH FORWARD AND REVERSE PROFILES
C
      WRITE(*,*)'PROVIDE THE 1ST LAYER VELOCITY'
      WRITE(*,*)
      READ(*,*)VI
C
C     PRINT INPUT CONTROL DATA
C
C
      CALL VAIT(NCH, NPT,NTRACE,DT,VSTRT,VSTOP,DV,X,TIT,TSTRT,VF2,TF2)
      WRITE(6,10) (TIT(I),I=1,20)
      WRITE(6,15)NCH,NPT,NTRACE
      WRITE(6,20)DT,VSTRT,VSTOP,DV
      WRITE(6,25)
      DO 105 I=1,NCH
105   WRITE(6,30)I,X(I),TSTRT(I)
      WRITE(6,32)VF2,TF2
      CALL VAIT (NCH,NPT,NTRACE,DT,VSTRT,VSTOP,DV,X,TIT,TSTRT,VR2,TR2)
      WRITE(6,10) (TIT(I),I=1,20)
      WRITE(6,15)NCH,NPT,NTRACE
      WRITE(6,20)DT,VSTRT,VSTOP,DV
      WRITE(6,25)
      DO 106 I=1,NCH
106   WRITE(6,30)I,X(I),TSTRT(I)
      WRITE(6,34)VR2,TR2
C
      IF(VR2-VF2)114,118,118
C
114   VU2=VF2
      VD2=VR2
      TU2=TF2
      TD2=TR2
      GO TO 102
```

```
116   VH=VF2
      TH=TF2
      GO  TO 102
118   VU2=VR2
      VD2=VF2
      TU2=TR2
      TD2=TF2
102   CONTINUE
C
C     COMPUTE ACTUAL LAYER VELOCITY(2), DEPTH(S) OF THE 1ST
C     INTERFACE(H1U & H1D) AND ANY LIKELY DIP OF THE LAYER(DIP1)
C
      XT=110.0
      PIE=3.141592654
      VUA=V1/VU2
      VDA=V1/VD2
C
      C12=ASIN(VUA)+ASIN(VDA))*0.5
C
      V2=V1/SIN(C12)
      H1U=(V1*TU2)/((2.0*COS(12))*1000.0)
      H1D=(V1*TD2)/((2.0*COS(C12))*1000.0)
C
      ARG=(H1U-H1D)/XT
C
      DIP1=ATAN(ARG)
      DIP1D=(DIP1*180.0)/PIE
C
      CALL VAIT(NCH,NPT,NTRACE,DT,VSTRT,VSTOP,DV,X,TIT,TSTRT,VF3,TF3)
      WRITE(6,10)(TIT(I),I=1,20)
      WRITE(6,15)NCH,NPT,NTRACE
      WRITE(6,20)DT,VSTRT.VSTOP,DV
      WRITE(6,25)
      DO 107 I=1,NCH
107   WRITE(6,30)I,X(I),TSTRT(I)
      WRITE(6,44)VF3,TF3
      CALL VAIT(NCH,NPT,NTRACE,DT,VSTRT,VSTOP,DV,X,TIT,TSTRT,VR3,TF3)
      WRITE(6,10)TIT(I),I=1,20)
      WRITE(6,15)NCH,NPT,NTRACE
      WRITE(6,20)DT,VSTRT,VSTOP,DV
      WRITE(6,25)
      DO 108 I=1,NCH
108   WRITE(6,30)I,X(I),TSTRT(I)
      WRITE(6,46)VR3,TR3
C
      IF(VR3-VF3)224,228,228
C
224   VU3=VF3
      VD3=VR3
      TU3=TF3
      TD3=TR3
      GO TO 202
226   VH3=VF3
      TH3=TF3
      GO TO 202
228   VU3=VR3
      VD3=VF3
      TU3=TR3
      TD3=TF3
```

```
202   CONTINUE
C
      VUB=V1/VU3
      VDB=V1/VD3
      C13D=ASIN(VUB)+DIPI
      C13U=ASIN(VDB)-DIP1
C
      VRA=V2/V1
      VSU=VRA*SIN(C13U)
      VSD=VRA*SIN(C13D)
      C23=0.5*(ASIN(VSU)+ASIN(VSD))
C
      DIP2=(0.5*((ASIN(VSU)-ASIN(VSD))+(2.0*DIP1)))
      DIP2D=(DIP2*180.0)/PIE
C
      HEU=(H1U*(COS(C13U)+COS(C13D)))/V1
      H2U=(V2*((TU3*0.001)-HEU))/(2.0*COS(C23))
      HED=(H1D*(COS(C13U)+COS(C13D)))/V1
      H2D=(V2*((TD3*0.001)-HED))/(2.0.*COS(C23))
C
      V3=V2/SIN(23)
C
      WRITE(6,48)V1
      WRITE(6,50)V2,V3
      WRITE(6,52)H1U,H2U
      WRITE(6,54)H1D,H2D
      WRITE(6,56)DIP1D,DIP2D
C
C WHERE V1,V2,V3, ARE VELOCITIES OF 1ST,2ND AND 3RD LAYERS RESPECTIVELY.
C H1U AND H2U ARE DEPTHS OF 1ST AND 2ND INTERFACES SHOOTING UPDIT;
C H1D AND H2D ARE DEPTHS OF 1ST AND 2ND INTERFACES SHOOTING DOWNDIP
C AND DIP1D AND DIP2D ARE DIPS OF 2ND AND 3RD LAYERS.
C
      STOP

10    FORMAT (1X,20A4/)
15    FORMAT(1X,'NO OF TRACES=',15,3X,'NO OF POINTs/BEAM=',15,3X,'N
     10 OF POINTS IN TRACE='15)
20    FORMAT(1X,'SAMPL.INT.=',F5,1,3X,'VSTRT,VSTOP=',2F8.1,3X,'VEL
     1 INCREMENT=',F5.1)
25    FORMAT(16X,'CHANNEL      DISTANCE    START  TIME')
30    FORMAT(16X,15,9X,F5.1,9X,F5.1)
32    FORMAT(14X,'2ND LAYER (F.PROF)VEL=',F6.1,1X,'TM INTER.=',F6.2///)
34    FORMAT(14X,'2ND LAYER(R.PROF)VEL=',F6.1,1X,'TM INTER.=',F6.2///)
44    FORMAT(14X,'3RD LAYER(F.PROF)VEL=',F6.1,5X,'TM INTER.=',F6.2///)
46    FORMAT(14X,'3RD LAYER(R.PROF)VEL=',F6.1,5X,'TM INTER =',F6.2///)
48    FORMAT(27X,'V1 =',F5.1/)
50    FORMAT(20X,'V2=',F6.1,5X,'V3=',F6.1/)
52    FORMAT(20X,'H1U =',F5.2,5X,'H2U =',F5.2/)
54    FORMAT(20X,'H1D =',F5.2,5X,'H2D =',F5.2/).
56    FORMAT(20X,'DIP1D=',F5.2,5X,'DIP2D=',F5.2/)
      END

      SUBROUTINE VAIT(NCH,NPT,NTRACE,DT,VSTRT,VSTOP,DV,X,
     *  TIT,TSTRT,VM,TI)
C
      DIMENSION CHA(12,200),CHT(12,200),TIT(20)
      DIMENSION TSTRT(12),BEAM(200),X(12)
      OPEN(UNIT=5,FILE='LDAT')
```

```
C
C     READ IN INPUT DATA
C
      READ(5,1)(TIT(I),I=1,20)
      READ(5,2)NCH,NPT,NTRACE
      READ(5,3)DT,VSTRT,VSTOP,DV
C
      DO 100 I=1, NCH
      READ(5,4)X(I),TSTRT(I)
100   CONTINUE
C
C     ZERO ALL CHANNELS
C
      V=VSTRT
      DO 100 I=1,NCH
      DO 110 J=1,NPT
110   CHA(I,J)=o.0
C
C     READ IN AND APPLY STEERING DELAYS TO DIGITIZED TRACES
C
      BEAMX=0.0
121   SIT=0.0
      D0125 I=1,NCH
      DO 125 J=1,NPT
125   CHT (I,J)=0.0
      DO 126 J=1,NPT
126   BEAM(J)=0.0
C
      DO 120 I=1,NCH
      NSTRT=IFIX((TSTRT(I)/DT)+0.5)
      NEND=NSTRT+NTRACE-1
      IF(V.GT.VSTRT)GO To 128
      READ(5,5)(CHA(I,J),J=NSTRT,NEND)
128   TCOR=(X(I)/V)*1000.0
      ICOR=IFIX((TCOR/DT)+0.5)
      DO 130 J=NSTRT,NPT
      K=J~ICOR
      CHT(I,K)=CHA(I,J)
130   CONTINUE
120   CONTINUE
C
      DO 140 I=1,NCH
      DO 140 J=1,NPT
      BEAM(J)=BEAM(J)+CHT(I,J)
140   CONTINUE
      BEAMP=0.0
      DO 150 J=1,NPT
      BEAM(J)=BEAM(J)/FLOAT(NCH)
150   BEAMP=BEAMP+(BEAM(J)*BEAM(J))
C
      IF(BEAMX.GE.BEAMP)GO TO 155
      BEMAX=BEAMP
      VM=V
C
      MM=o
152   MM=MM+1
      DO 153 J=MM,NPT
      TNE=0.0
```

```
      IF(ABS(BEAM(J)).GT.0.0)GO TO 200
153   CONTINUE
C
200   INTER=J
      INEND=INTER+5
C
210   INEG=INTER+1
      DO 220 K=INEG,INEND
      IF(BEAM(K).EQ.0.0.OR.BEAM(K).GT.0.0)GO TO 152
220   CONTINUE
      TNE=FLOAT(INTER)
      GO TO 500
C
250   INPOS=INTER+1
      DO 270 KK=INPOS,INEND
      IF(BEAM(KK).EQ.0.00R.BEAM(KK).LT.0.0)GO TO 152
270   CONTINUE
      TPO=FLOAT(INTER)
500   TI=TNE+TPO
C
155   V=V+DV
      IF(VSTOP-V)160,121,121
160   CONTINUE
C
1     FORMAT(20A4)
2     FORMAT(315)
3     FORMAT(F5.1,1X,F6.1,1X,F6.1,1X,F5.1)
4     FORMAT(F5.1,1X,F5.1)
5     FORMAT(10F8.1)
C
      RETURN
      END
```

Appendix B

```
      SUBROUTINE  SETRAN
      COMMON I, J, K, M
C
      I = 0
      J = 3612
      K = 5701
      M = 566927
C
      RETURN
      END
C
C
      FUNCTION RAN
      COMMON I,J,K,M
C
      I = MOD (I*J+K,M)
      RAN = (FLOAT (I)/FLOAT(M) )
C
      RETURN
      END
```

Appendix C

```
      PROGRAM  QUANTNOISE
      DIMENSION CHT(12,100), BN(100), CHA (1000)
      OPEN(UNIT=6,FILE = 'OUTPUT')
C
      NPT = 100
      CALL SETRAN
      DO 100 I = 1 1000
      DET = (FLOAT(I) *6.0) - 6.0
      CHA (I) = RAN (DET)
1000  CONTNUE
C
      DO  800  KK = 1, 12
      NCH = KK
      K = 1
      DO 300 I = 1 NCH
      DO 200 J = K, NPT
      CHT (I,J) = CHA (J)
200   CONTINUE
      K = K + NPT
300   CONTINUE
C
      DO 400 J = 1, NPT
400   BN (J) = 0.0
C
      EBN = 0.0
C
      DO 500 I = 1, NU+
      DO 500 J = 1, NPT
500   BN(J) = BN(J) + CHT (I,J)
C
      DO 600 J = 1, NPT
600   EBN = EBN + (BN (J) **2)
C
      WRITE(6,700) KK,EBN
700   FORMAT (15x,I2,6x, F8.4)
800   CONTINUE
      STOP
      END
```

A P P E N D I X 'D'

MANUAL T-X PLOTS

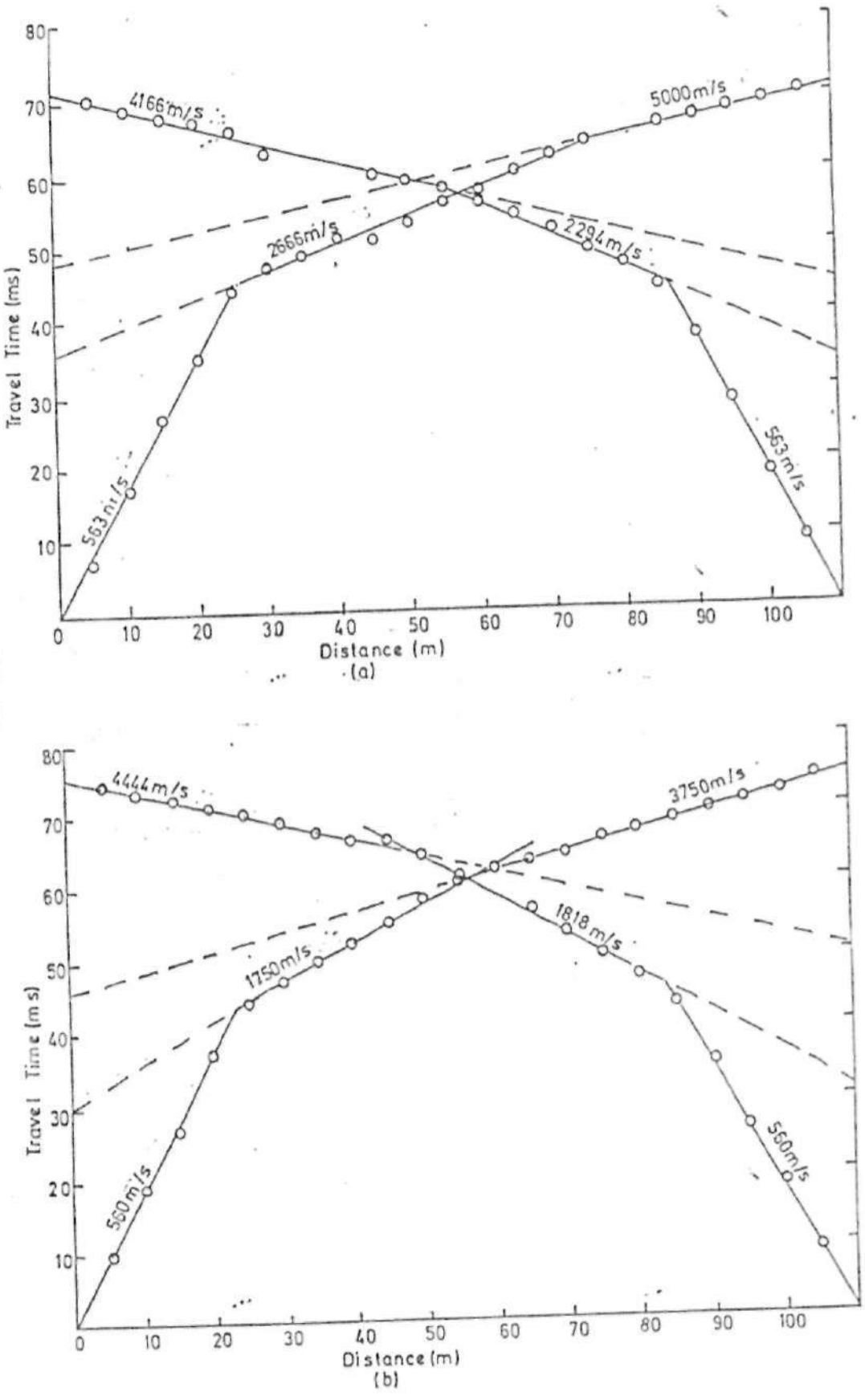


Fig.D.1 (a) and (b): Manual T-X Plots of the field data for spreads 1 & 2 profile S-S'

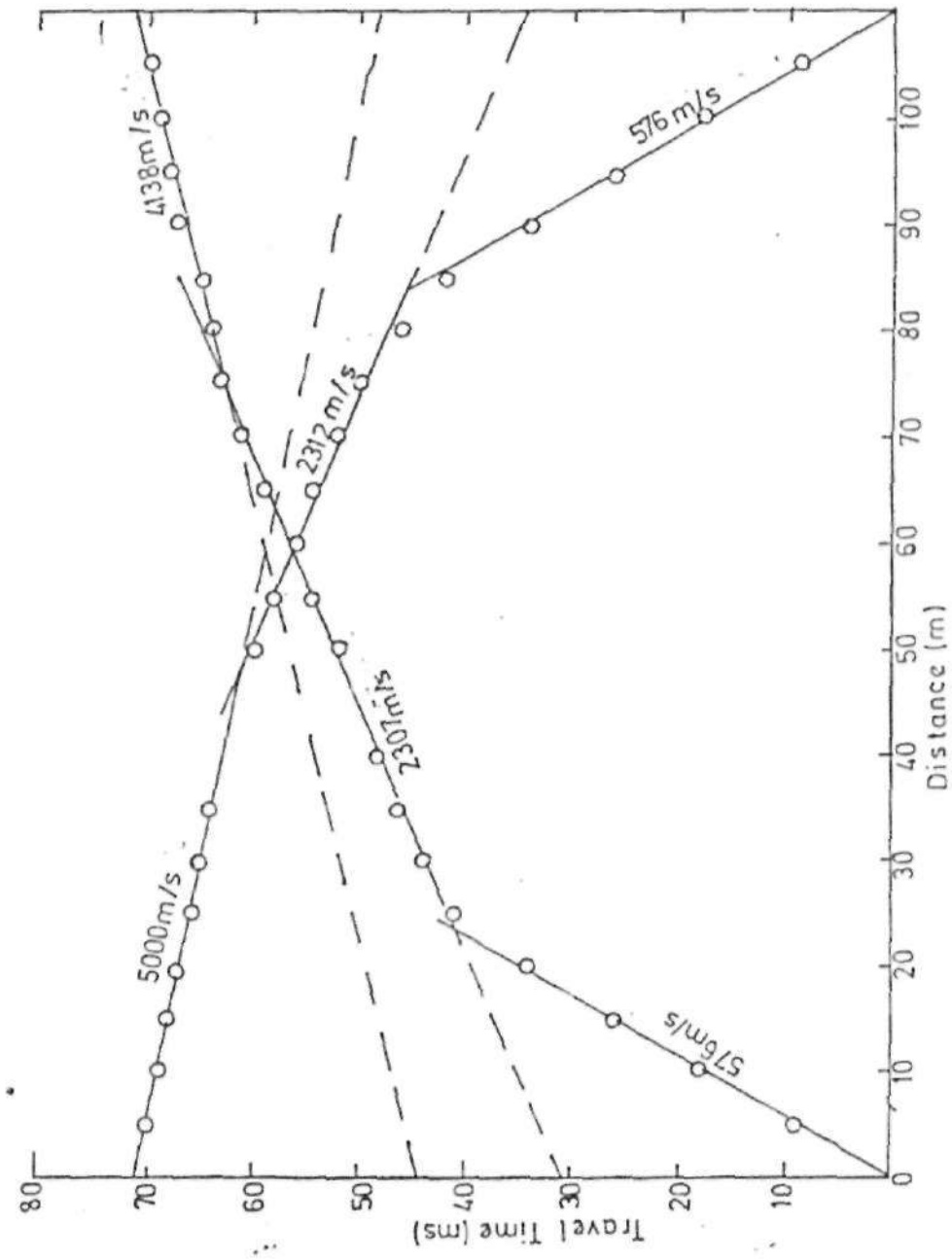


Fig. D.1 (c): Manual T-X plot of the field data for spread 3 of profile S-S'

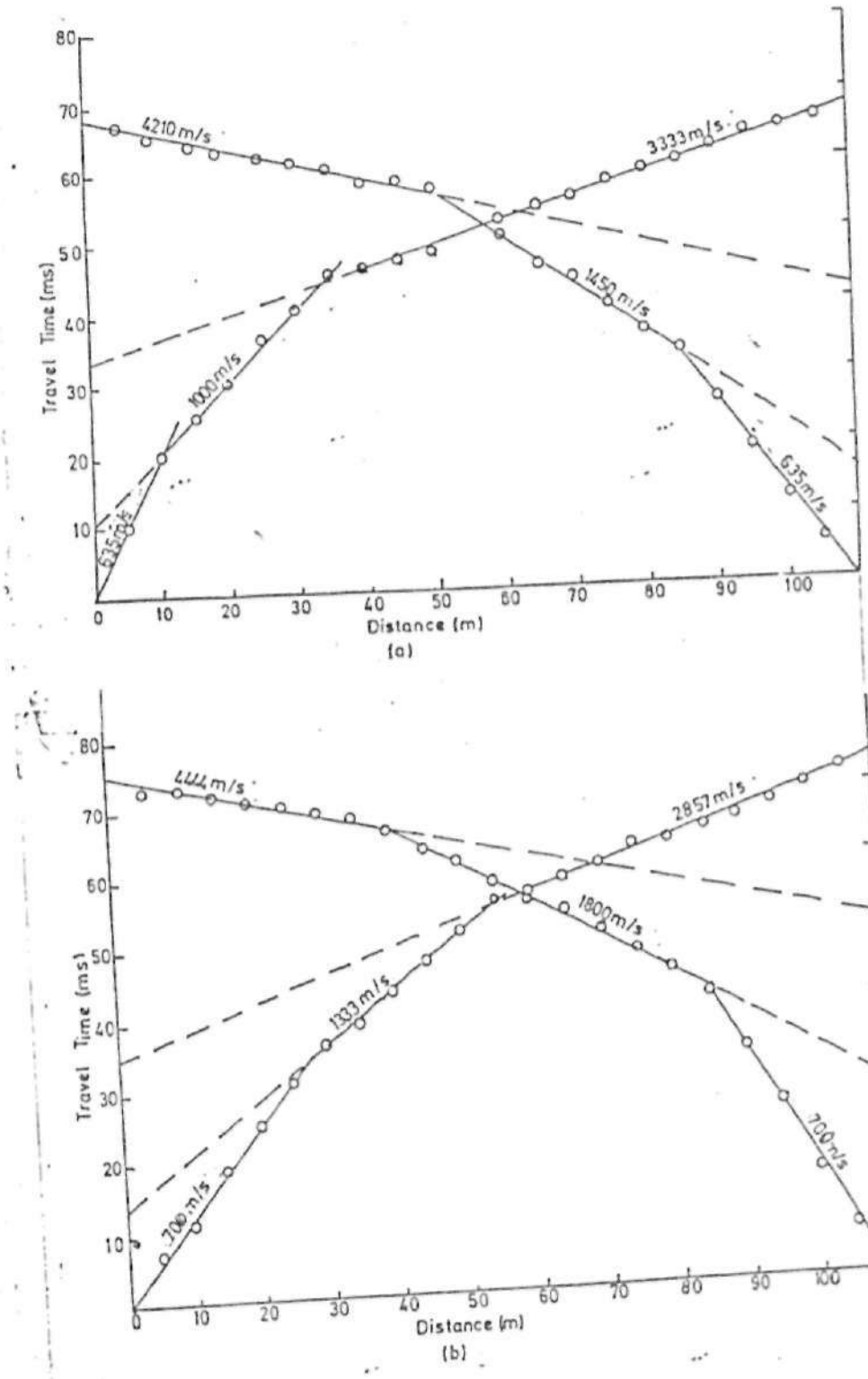


Fig. D.2 (a) & (b): Manual T-X plots of the field data for spreads 1 & 2 of profile SS-SS'

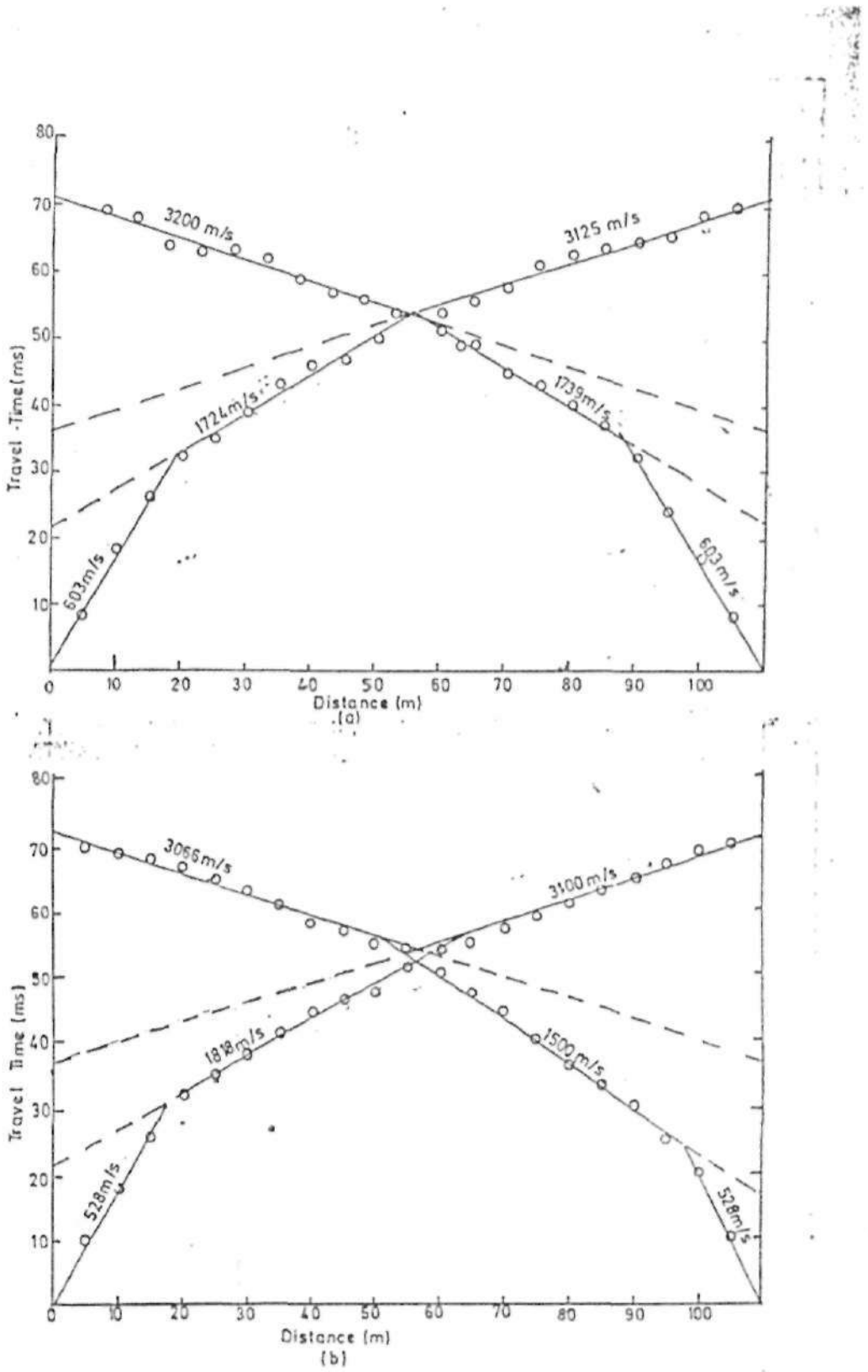


Fig. D.3 (a) & (b): Manual T-X plots of the field data for spreads 1 & 2 of profile H-H'

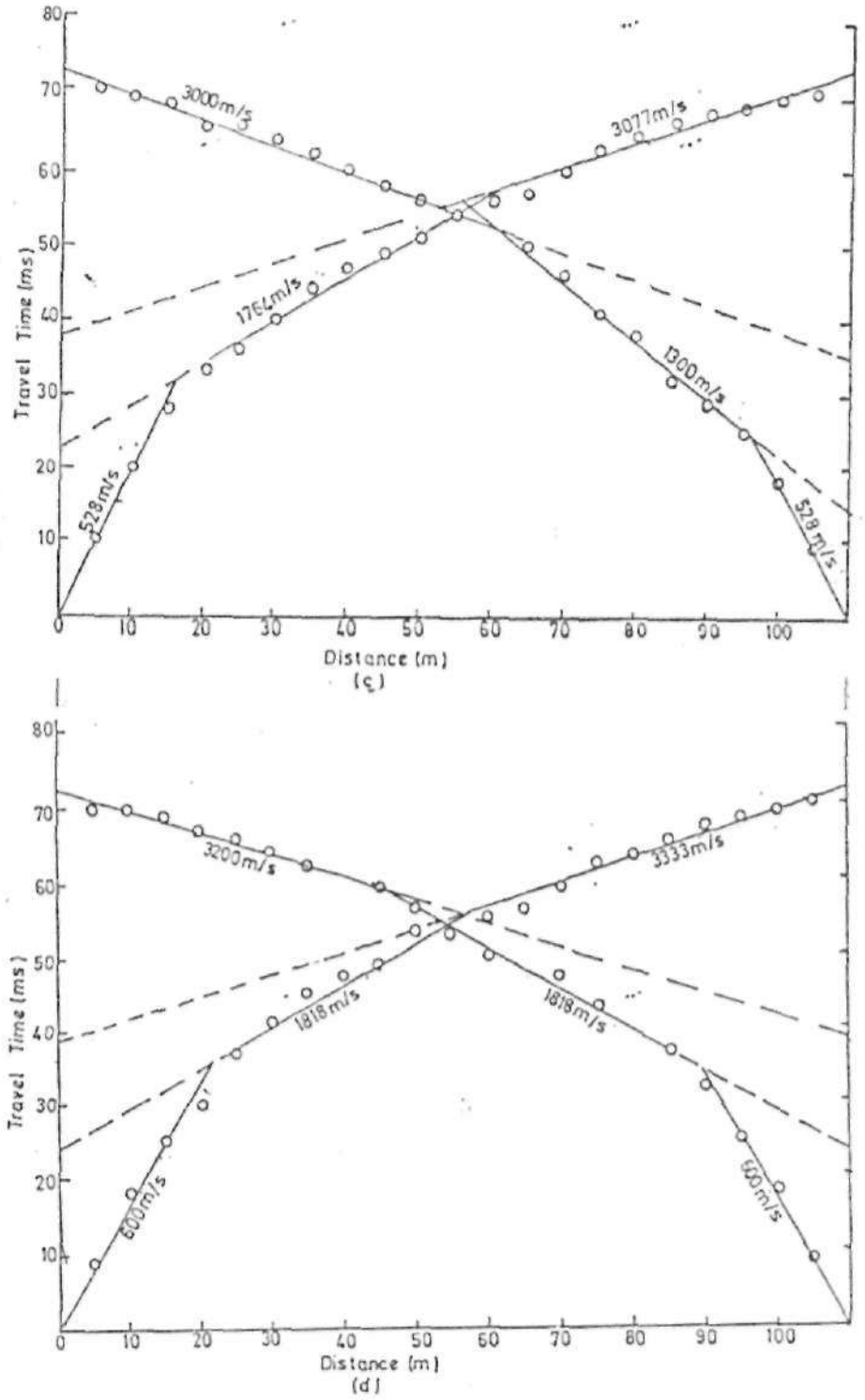


Fig. D.3 (c) & (d): Manual T-X plots of the field data for spreads 3 & 4 of profile H-H'

314016

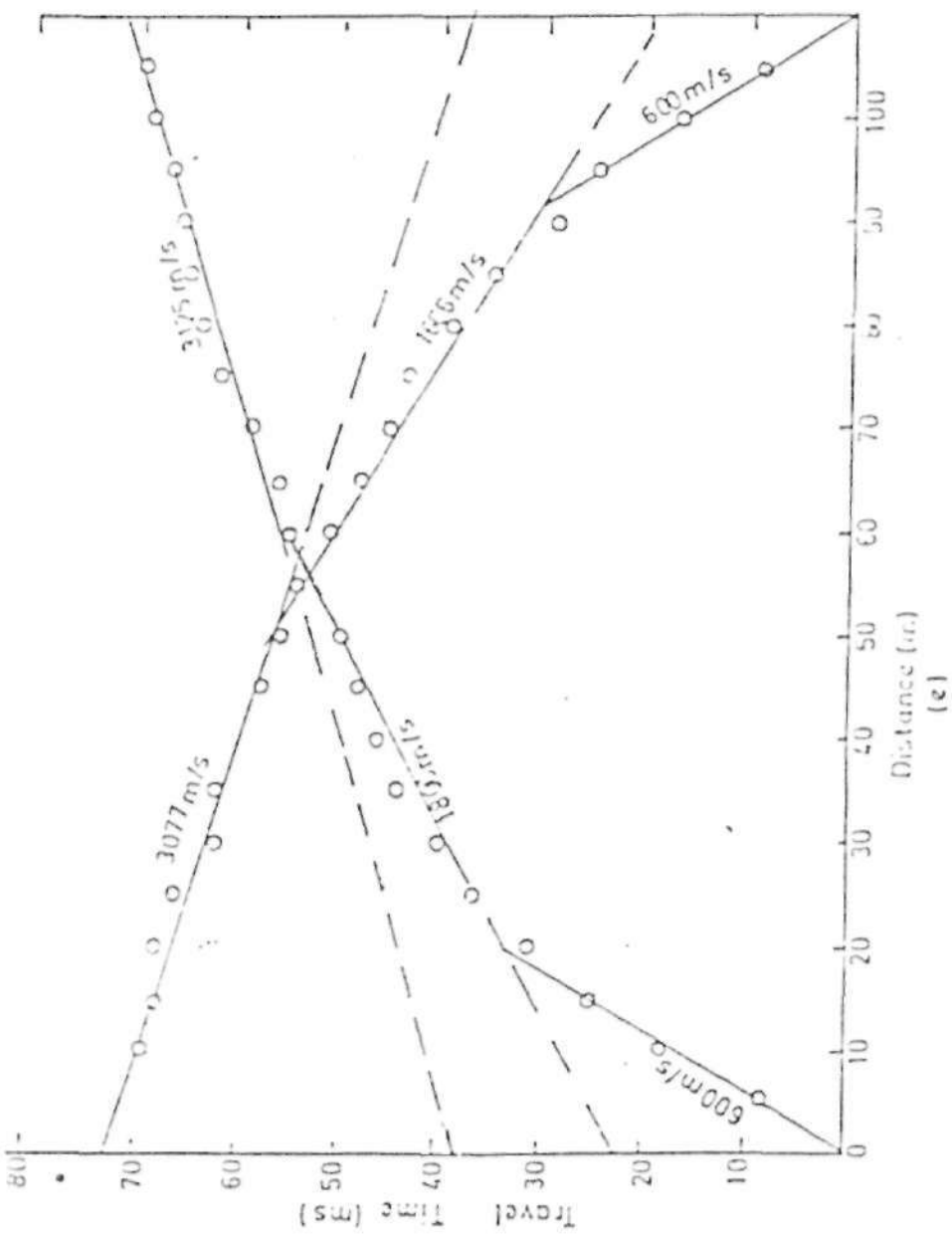


Fig. D.3 (e): Manual T-X plot of the field data for spread 5 of profile H-H'.